nature biomedical engineering

ARTICLES

https://doi.org/10.1038/s41551-020-0563-4

Check for updates

Pharmacokinetic tuning of protein–antigen fusions enhances the immunogenicity of T-cell vaccines

Naveen K. Mehta[1,2], Roma V. Pradhan[2], Ava P. Soleimany[1,3], Kelly D. Moynihan[1,2,4], Adrienne M. Rothschilds[1,2], Noor Momin[1,2], Kavya Rakhra[1], Jordi Mata-Fink[4,5], Sangeeta N. Bhatia[1,2,6,7,8,9,11], K. Dane Wittrup[1,2,5] ✉ and Darrell J. Irvine[1,2,4,10,11] ✉

The formulations of peptide-based antitumour vaccines being tested in clinical studies are generally associated with weak potency. Here, we show that pharmacokinetically tuning the responses of peptide vaccines by fusing the peptide epitopes to carrier proteins optimizes vaccine immunogenicity in mice. In particular, we show in immunized mice that the carrier protein transthyretin simultaneously optimizes three factors: efficient antigen uptake in draining lymphatics from the site of injection, protection of antigen payloads from proteolytic degradation and reduction of antigen presentation in uninflamed distal lymphoid organs. Optimizing these factors increases vaccine immunogenicity by up to 90-fold and maximizes the responses to viral antigens, tumour-associated antigens, oncofetal antigens and shared neoantigens. Protein–peptide epitope fusions represent a facile and generalizable strategy for enhancing the T-cell responses elicited by subunit vaccines.

In recent years, immunotherapies have transformed clinical oncology, including checkpoint blockade antibodies[1–3], chimeric antigen-receptor T cells[4,5], bispecific T-cell engagers[6] and oncolytic viruses[7]. However, vaccines—the oldest and most-studied form of immunological intervention—have had only modest clinical success, with a single FDA approval to date[8], despite their theoretical potential to enhance the response rates of checkpoint inhibitors[9–11]. Peptide vaccines in particular have been a focus in many recent cancer therapy trials, due in part to their safety, modest cost and capacity to be rapidly manufactured, enabling patient-specific neoantigen vaccines[12,13]. However, the potency of peptide vaccines remains poor, especially in humans.

A number of pharmacokinetic shortcomings of peptide vaccines have been well characterized, including inefficient antigen transport to local draining lymph nodes (dLNs)[14,15] and proteolytic instability[16,17]. Delivery strategies have been developed to address these limitations, including the formulation of peptide antigens in synthetic particles[18–20], antibody-mediated targeting of antigen to dendritic cells[21,22] and direct intra-nodal injections[23,24] to obviate the need for antigenic trafficking altogether. Although effective, these approaches are complex in terms of manufacturing and/or administration, motivating the development of additional solutions.

Here we report the role of vaccine antigen pharmacokinetics in controlling the potency of subunit vaccines and define strategies to optimize vaccine potency via pharmacokinetic tuning of antigen delivery. To control antigen degradation rates and pharmacokinetics, we fused tumour-associated epitopes to minimally immunogenic protein carriers. By varying the identity of the carrier protein, we systematically altered the pharmacokinetic and biodistribution characteristics of the fusions to define key factors controlling vaccine potency. We find that immunogenicity is maximized by employing carrier proteins that exhibit prolonged residence time in local adjuvant-inflamed dLNs but short half-lives in systemic circulation, minimizing uptake in distal uninflamed lymphoid organs. Collectively, these conclusions help identify a set of simple pharmacokinetic design criteria to aid in the engineering of molecular vaccines.

Results

Fusion of peptide antigens to albumin enhances lymphatic uptake. Following parenteral injection, antigens can be absorbed into systemic circulation, degraded in tissue, trafficked into lymph or captured by antigen-presenting cells (APCs) locally. We hypothesized that fusion of peptide antigens to a bulky protein carrier could limit these first two potential fates to promote immune priming. The levels of antigen in the blood following subcutaneous injection are a function of the systemic absorption rate (k_{abs}) and the rate of clearance from circulation (k_{clear}), which collectively determine antigen bioavailability in both the dLNs and distal lymphoid organs (Fig. 1a). Previous work has shown that parenterally administered molecules <40 kDa in size are systemically absorbed through capillary endothelial cell junctions, whereas larger molecules are size-excluded from entering the blood vasculature and instead drain to lymphatic vessels[15,25], motivating the commonly implemented strategy of delivering low-molecular-weight vaccine components in larger particulate formulations[18–20]. To determine the hydrodynamic size threshold for efficient lymphatic uptake in mice, we first assessed the accumulation of dextrans of various molecular weights

[1]Koch Institute for Integrative Cancer Research, Massachusetts Institute of Technology, Cambridge, MA, USA. [2]Department of Biological Engineering, Massachusetts Institute of Technology, Cambridge, MA, USA. [3]Harvard Graduate Program in Biophysics, Harvard University, Boston, MA, USA. [4]The Ragon Institute of Massachusetts General Hospital, Massachusetts Institute of Technology and Harvard University, Cambridge, MA, USA. [5]Department of Chemical Engineering, Massachusetts Institute of Technology, Cambridge, MA, USA. [6]Harvard–MIT Health Sciences and Technology Program, Institute for Medical Engineering and Science, Massachusetts Institute of Technology, Cambridge, MA, USA. [7]Department of Electrical Engineering and Computer Science, Massachusetts Institute of Technology, Cambridge, MA, USA. [8]Department of Medicine, Brigham and Women's Hospital, Harvard Medical School, Boston, MA, USA. [9]Broad Institute of Massachusetts Institute of Technology and Harvard, Cambridge, MA, USA. [10]Department of Materials Science and Engineering, Massachusetts Institute of Technology, Cambridge, MA, USA. [11]Howard Hughes Medical Institute, Cambridge, MA, USA. ✉e-mail: wittrup@mit.edu; djirvine@mit.edu

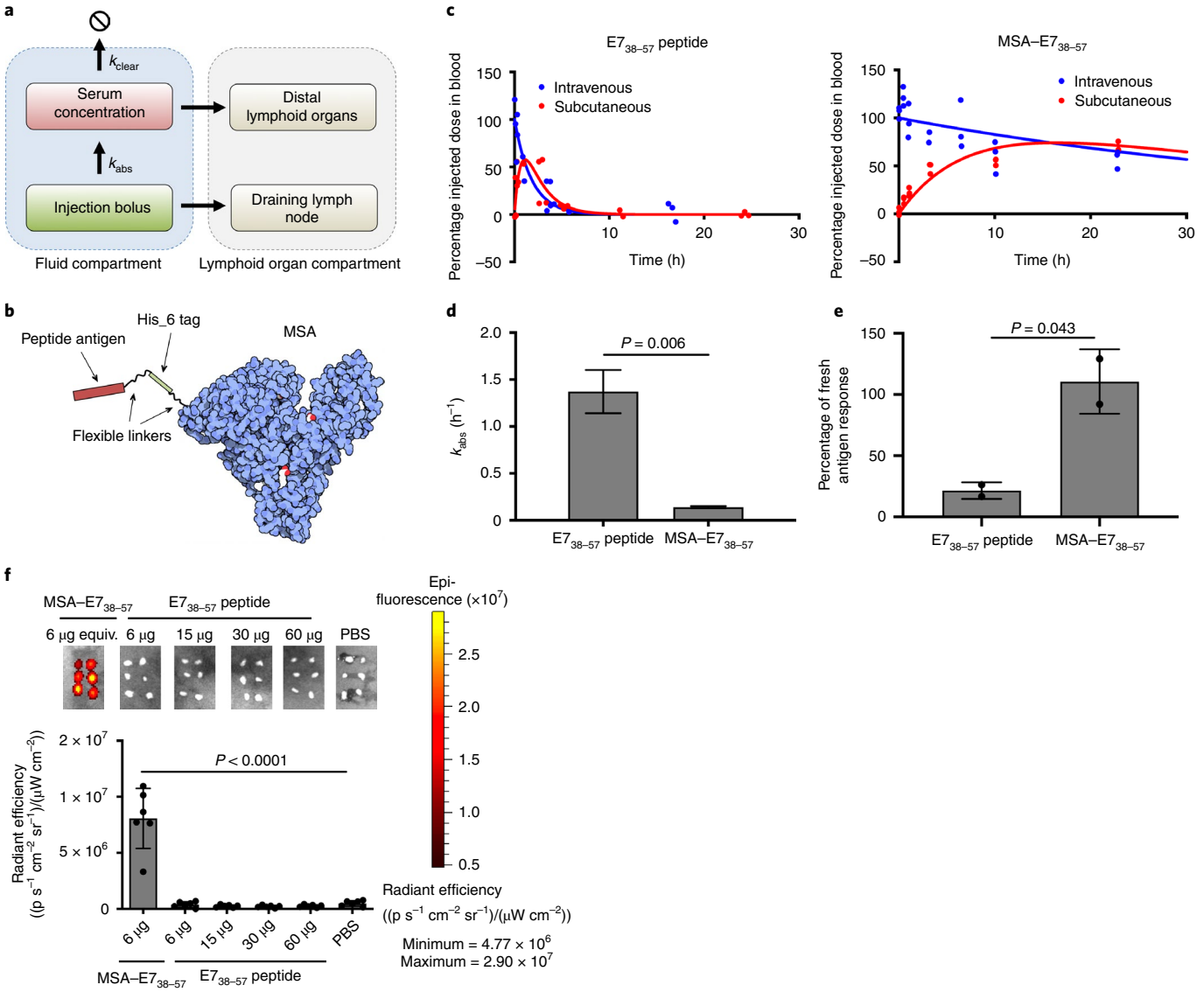

Fig. 1 | Albumin fusion enhances the bioavailability of antigen in the dLN. a, Pharmacokinetic model describing the absorbance rate (k_{abs}) and clearance rate (k_{clear}), which determine bioavailability in lymphoid organs. **b**, Schematic of the MSA–$E7_{38-57}$ protein design. **c**, FITC-labelled $E7_{38-57}$ or MSA–$E7_{38-57}$ were either subcutaneously or intravenously injected in mice ($n = 3$ mice per group). Blood draws of <10 µl were used to quantify the antigen concentration in serum over the course of 24 h following injection; data were used to determine the pharmacokinetic model fits, shown as solid lines. **d**, Calculated k_{abs} values for the $E7_{38-57}$ peptide and MSA–$E7_{38-57}$ (fit data ± standard error). **e**, Splenocytes from the mice vaccinated with $E7_{38-57}$ were restimulated in the presence of brefeldin A with the indicated antigen, either fresh or treated with 10% mouse serum for 24 h. The percentage IFN-γ response from serum-treated antigen restimulation compared with the response to fresh antigen, measured by ICS, is shown ($n = 2$ replicates). **f**, FITC-labelled $E7_{38-57}$ or MSA–$E7_{38-57}$ were injected subcutaneously in mice at the indicated doses. Inguinal lymph nodes were excised and imaged through IVIS 8 h after injection ($n = 6$ lymph nodes per group). Data are representative of two independent experiments; equiv., equivalent. **d**–**f**, Statistical significance was calculated using two-tailed Student's *t*-tests (**d**,**e**) or one-way analysis of variance (ANOVA) with Dunnett's multiple comparisons test versus the PBS group (**f**).

in lymph nodes. Consistent with previous findings, while 4 kDa dextran (hydrodynamic radius of 1.2 nm) did not access the dLN above background, dextrans over 20 kDa (radius ≥ 2.4 nm) did so effectively (Supplementary Fig. 1a,b).

Based on these data, we hypothesized that peptide epitopes (~2 kDa) would have low lymphatic uptake due to high k_{abs} values, which could be reversed by fusing antigen to mouse serum albumin (MSA, 69 kDa)—a highly stable and easily expressed protein with a hydrodynamic radius of 3.3 nm (Supplementary Fig. 1a). To test this idea, we fused a long peptide from human papillomavirus (HPV) $E7_{38-57}$, containing the H-2D^b-restricted CD8$^+$ T-cell epitope $E7_{49-57}$, to the carboxy (C) terminus of MSA[26] (Fig. 1b). MSA–$E7_{38-57}$ was expressed in HEK cells and purified without evidence of contaminants or aggregation (Supplementary Fig. 2a). To determine the k_{abs} for this antigen fusion, we subcutaneously injected mice with fluorescein isothiocyanate (FITC)-labelled MSA–$E7_{38-57}$ or free $E7_{38-57}$ peptide and measured the percentage of injected dose in their blood over time (Fig. 1c). These measurements revealed that the k_{abs} was greatly reduced for MSA–$E7_{38-57}$ compared with free peptide (0.14 h^{-1} versus 1.37 h^{-1}, respectively; Fig. 1d).

In addition to rapid systemic absorption, peptides suffer from proteolytic instability[16,17]. To assess whether MSA fusion could protect the peptide from degradation, we restimulated splenocytes from mice vaccinated with $E7_{38-57}$ ex vivo with either fresh or

serum-treated $E7_{38-57}$ antigens and measured interferon-γ (IFN-γ) production by intracellular cytokine staining (ICS). Ex vivo splenocyte recall in response to free $E7_{38-57}$ peptide was reduced by 78% when the peptide was serum-treated, whereas stimulation by MSA–$E7_{38-57}$ was minimally affected by serum exposure (Fig. 1e). As a more direct measure of proteolysis, $E7_{38-57}$ peptides and MSA fusions were prepared with His_6 and FLAG tags flanking the amino (N)- and C-terminal ends of the epitope, and a sandwich ELISA was performed to detect cleavage of the $E7_{38-57}$ epitope following incubation in 20% mouse plasma (Supplementary Fig. 3a); 34% of the free $E7_{38-57}$ was cleaved in 4 h, whereas MSA–$E7_{38-57}$ remained fully intact over this time course (Supplementary Fig. 3b).

One potential disadvantage of the protein-fusion strategy is that proteins poorly target the cytosolic antigen presentation pathway, which hinders their immunogenicity. However, despite protection from extracellular proteases, we found that MSA-fused epitopes are more readily processed than epitopes buried within the polypeptide chain, as MSA–$Ova_{251-270}$ could stimulate OTI splenocytes more potently than intact Ova protein (Supplementary Fig. 4). Displaying epitopes on the terminal end of MSA protects epitopes from serum degradation while preserving bioactivity in APCs.

Due to its appropriate size and improved proteolytic stability, FITC-labelled MSA–$E7_{38-57}$ effectively trafficked to the dLN following subcutaneous administration, whereas labelled $E7_{38-57}$ peptide failed to accumulate above background, as measured by IVIS imaging, even at tenfold-higher molar doses (Fig. 1f). Notably, administration of peptide in the commonly used Montanide water-in-oil emulsion adjuvant also failed to improve dLN bioavailability (Supplementary Fig. 5a) and instead led to retention at the injection site (Supplementary Fig. 5b), a phenomenon previously reported to lead to anergy/deletion of responding T cells[27]. Collectively, we conclude that expression as a fusion to MSA substantially improves antigen delivery to dLNs.

Albumin fusions potentiate cellular immune responses. To test the immunogenicity of MSA–$E7_{38-57}$ relative to free $E7_{38-57}$ peptide, mice were subcutaneously primed and boosted 14 d later with $E7_{38-57}$ or MSA–$E7_{38-57}$ mixed with cyclic di-GMP, a cyclic dinucleotide (CDN) STING agonist[28], as an adjuvant. H-$2D^b$–$E7_{49-57}$ tetramer staining 6 d post-boost revealed that MSA fusions elicited 49-fold higher frequencies of $E7_{49-57}$-specific $CD8^+$ T cells in blood compared with vaccination with the $E7_{38-57}$ peptide (Fig. 2a). Even tenfold-higher doses of the $E7_{38-57}$ peptide failed to replicate the immunogenicity of the albumin–antigen fusion protein (Fig. 2b). Importantly, antibodies were not raised against MSA (Supplementary Fig. 6a,b) and MSA-fusion vaccination elicited memory T cells that rejected a tumour challenge two months after vaccination (Supplementary Fig. 7). Furthermore, MSA–$E7_{38-57}$ outperformed $E7_{38-57}$ when paired with a panel of adjuvants including CpG (a TLR9 agonist), polyinosinic:polycytidylic acid (poly(I:C); a TLR3 agonist) and lipo-CpG (a potent lymph node-targeting variant of CpG[14]; Fig. 2c). MSA–$E7_{38-57}$ fusions could also elicit therapeutic T-cell responses against established subcutaneous $E7^+$ TC-1 tumours. Following weekly vaccination, the mice that were treated with MSA–$E7_{38-57}$ had a statistically significant improvement in tumour control relative to PBS-treated mice as well as a 40% cure rate, whereas the median survival of the mice treated with $E7_{38-57}$ was unchanged relative to untreated animals and only 10% of these mice were cured (Fig. 2d).

The generalizability of the MSA-peptide fusion vaccine was assessed by attaching other tumour-associated epitopes, including $Trp1_{1455-1463}$ altered peptide ligand (APL)[29], $gp100_{20-39}$ APL[30] and oncofetal antigen $CEA_{567-584}$ (ref. [31]). Following prime and boost vaccination, ICS was used to measure IFN-γ and tumour necrosis factor-α (TNF-α) in peripheral blood mononuclear cells (PBMCs) after ex vivo stimulation with the appropriate peptide antigen. As measured by IFN-γ^+CD8^+ T cells, MSA–epitope fusion vaccines outperformed their peptide counterparts by 18-fold for $Trp1_{1455-1463}$ APL, 39-fold for $gp100_{20-39}$ APL and 61-fold for $CEA_{567-584}$ (Fig. 2e). Mouse serum albumin-fusion vaccines, but not peptide vaccines, also generated polyfunctional IFN-γ^+TNF-α^+CD8^+ T-cell responses.

In *Batf3*$^{-/-}$ mice, which lack cross-presenting Batf3-dependent dendritic cells (DCs), MSA–$E7_{38-57}$ immunogenicity was reduced by 70% in a prime–boost vaccination study (Supplementary Fig. 8a), and MSA–$E7_{38-57}$ ineffectively treated TC-1 tumours in *Batf3*$^{-/-}$ mice (Supplementary Fig. 8b,c). To test whether DC targeting would further enhance the immunogenicity of albumin fusions, we utilized yeast surface display to engineer a fibronectin clone (DEC1) that bound DEC-205, an internalizing receptor expressed on DCs, with a dissociation constant (K_d) of 0.66 nM (Supplementary Fig. 8d). DEC1 was fused to the N-terminal end of MSA–$E7_{38-57}$ (DEC1–MSA–$E7_{38-57}$). Immunization with DEC1–MSA–$E7_{38-57}$ increased lymph node-resident $CD8^+$ DC uptake of antigen by 39-fold compared with MSA–$E7_{38-57}$, although the total dLN accumulation was unaffected (Supplementary Fig. 8e,f). However, as an immunogen, DEC1–MSA–$E7_{38-57}$ elicited T-cell responses that did not statistically differ from MSA–$E7_{38-57}$ over a broad dose range (Supplementary Fig. 8g). Thus, at least for albumin-fusion antigens, we find that specific APC targeting does not further improve T-cell responses. The fact that MSA–$E7_{38-57}$ can elicit strong immune responses dependent on cross-presentation (Supplementary Fig. 8a) despite relatively poor, but non-zero, $CD8^+$ DC uptake (Supplementary Fig. 8c) suggests that even low quantities of antigen accumulation in the right APC population can drive robust immunity.

Systemic antigen exposure promotes tolerance. Because persistent antigen presentation in the absence of inflammatory cues can induce T-cell tolerization and dysfunction[27,32–34], we hypothesized that the long circulating half-life of MSA–$E7_{38-57}$ (36 h) may prolong antigen presentation in poorly inflamed distal lymphoid organs. In fact, we found that intravenously administered MSA–$E7_{38-57}$ mixed with CDN failed to prime a cellular immune response (Fig. 3a). Mice that were administered a single intravenous injection of MSA–$E7_{38-57}$, with or without adjuvant, were instead tolerized against a subsequent subcutaneous prime–boost challenge. We observed a >85% drop in the magnitude of the T-cell response compared with animals that had received a control intravenous injection of PBS before the challenge (Fig. 3b). Notably, intravenous tolerization via MSA–$E7_{38-57}$ was significantly more effective than intravenous administration of the $E7_{38-57}$ peptide, a strategy that is commonly used to induce tolerance[35,36] (Fig. 3c).

To assess the kinetics of antigen presentation relative to inflammatory cues in different tissue sites, we subcutaneously vaccinated mice with MSA–$gp100_{20-39}$ and CDN adjuvant. After 1, 4 or 7 d, 5×10^5 $Thy1.1^+$ pmel cells expressing T-cell receptors (TCRs) specific to the gp100 epitope were adoptively transferred into vaccinated animals to serve as reporters of antigen presentation. The local dLN (inguinal node) and distal lymphoid organs (mesenteric nodes and spleen) were excised 24 h later, and resident Thy1.1 cells were assessed for CD69 expression indicative of TCR triggering. $CD8^+$ DCs were analysed for CD86 expression indicative of DC activation at equivalent time points. Consistent with previous reports of rapid CDN clearance[37], $CD8^+$ DCs were poorly activated in distal organs; instead, only the local dLN was inflamed. Nonetheless, antigen presentation persisted in distal uninflamed organs: CD69 was still upregulated on pmel T cells in the mesenteric lymph nodes when transferred 4 d after immunization or in the spleen when transferred 7 d after immunization (Fig. 3d). While the local dLN probably contributes to activating immunity due to the simultaneous presence of both antigen and inflammatory cues, persistent antigen presentation in the absence of DC activation in distal organs may blunt functional immunity.

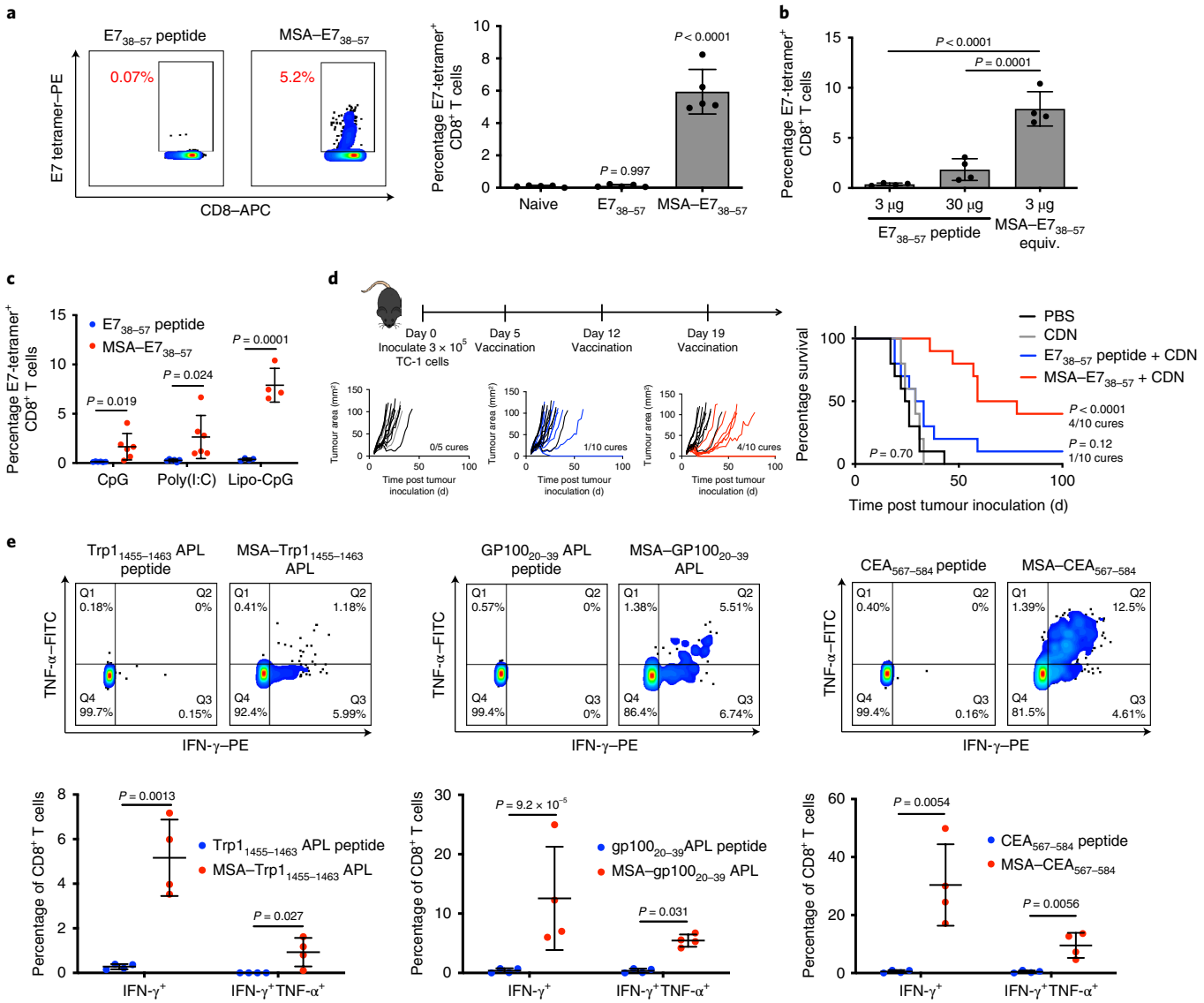

Fig. 2 | Albumin delivery of epitopes is a generalizable immunogenicity enhancement strategy. a, Mice were subcutaneously primed and boosted with either $E7_{38-57}$ or MSA-$E7_{38-57}$ and CDN. Representative tetramer-stain flow plots of $CD8^+$ T cells 6 d after boost (left) and quantification (right; mean ± s.d.; $n = 5$ mice per group). Data are representative of over five independent experiments. **b**, Mice were primed and boosted with $E7_{38-57}$ or MSA-$E7_{38-57}$ as in **a** at the indicated doses. Tetramer-stain data of $CD8^+$ T cells 6 d after the boost are shown (mean ± s.d.; $n = 4$ mice per group). **c**, Mice were subcutaneously primed and boosted with $E7_{38-57}$ or MSA-$E7_{38-57}$ and the indicated adjuvants. Tetramer-stain data of CD8+ T cells 6 d after the boost are shown (mean ± s.d.; $n = 6$ mice per group for CpG and poly(I:C) and $n = 4$ mice for lipo-CpG). **d**, Timeline and treatment schematic of the TC-1 tumour study (top left), along with tumour growth plots (bottom left) and survival curves (right; $n = 5$ mice for CDN and $n = 10$ mice for all other groups). Data are compiled from two independent experiments. **e**, Mice were primed and boosted with the indicated antigens as in **a**. Six days after the boost, peripheral blood cells were stimulated with WT optimal antigenic peptides for 6 h in the presence of brefeldin A. Representative flow cytometry plots for ICS of $CD8^+$ T cells (top) and quantification (bottom; mean ± s.d.; $n = 4$ mice per group). Statistical significance was calculated using a one-way ANOVA with Dunnett's multiple comparisons test versus the naive group (**a**), one-way ANOVA with Tukey's multiple comparisons test between all groups (**b**), two-tailed Student's *t*-tests between groups on the *x* axis with Holm–Sidak's multiple comparisons test (**c**,**e**) or two-tailed log-rank (Mantel–Cox) test versus the PBS group (**d**).

To more specifically query the mechanisms of tolerance following systemic exposure to albumin fusions in the absence of adjuvant, we transferred 1×10^6 $Thy1.1^+$ pmel cells into recipient mice and subsequently intravenously administered PBS, $gp100_{20-39}$ peptide or MSA–$gp100_{20-39}$ without adjuvant. Subcutaneous administration of MSA–$gp100_{20-39}$ with adjuvant was used as a control for activating immunity. While MSA–$gp100_{20-39}$ delivery both with and without adjuvant induced $Thy1.1^+$ cell expansion by day 3, expansion continued through day 7 only in response to MSA–$gp100_{20-39}$ with adjuvant; without adjuvant, the $Thy1.1^+$ cells were rapidly deleted by day 7 (Fig. 3e). $Thy1.1^+$ cells from the inguinal lymph node, where the activating vaccine triggers functional immune responses, were further immunophenotyped. Only $Thy1.1^+$ cells from mice that received MSA–$gp100_{20-39}$ without adjuvant had elevated populations of $PD1^+Lag3^+$ and $PD1^+Tim3^+$ cells over the background (Fig. 3f), and $Thy1.1^+$ cells from mice that received tolerizing vaccines exhibited deficiencies in cytokine production following ex vivo recall (Fig. 3g). $CD8^+$ T cells that express Foxp3 are emerging as an important class

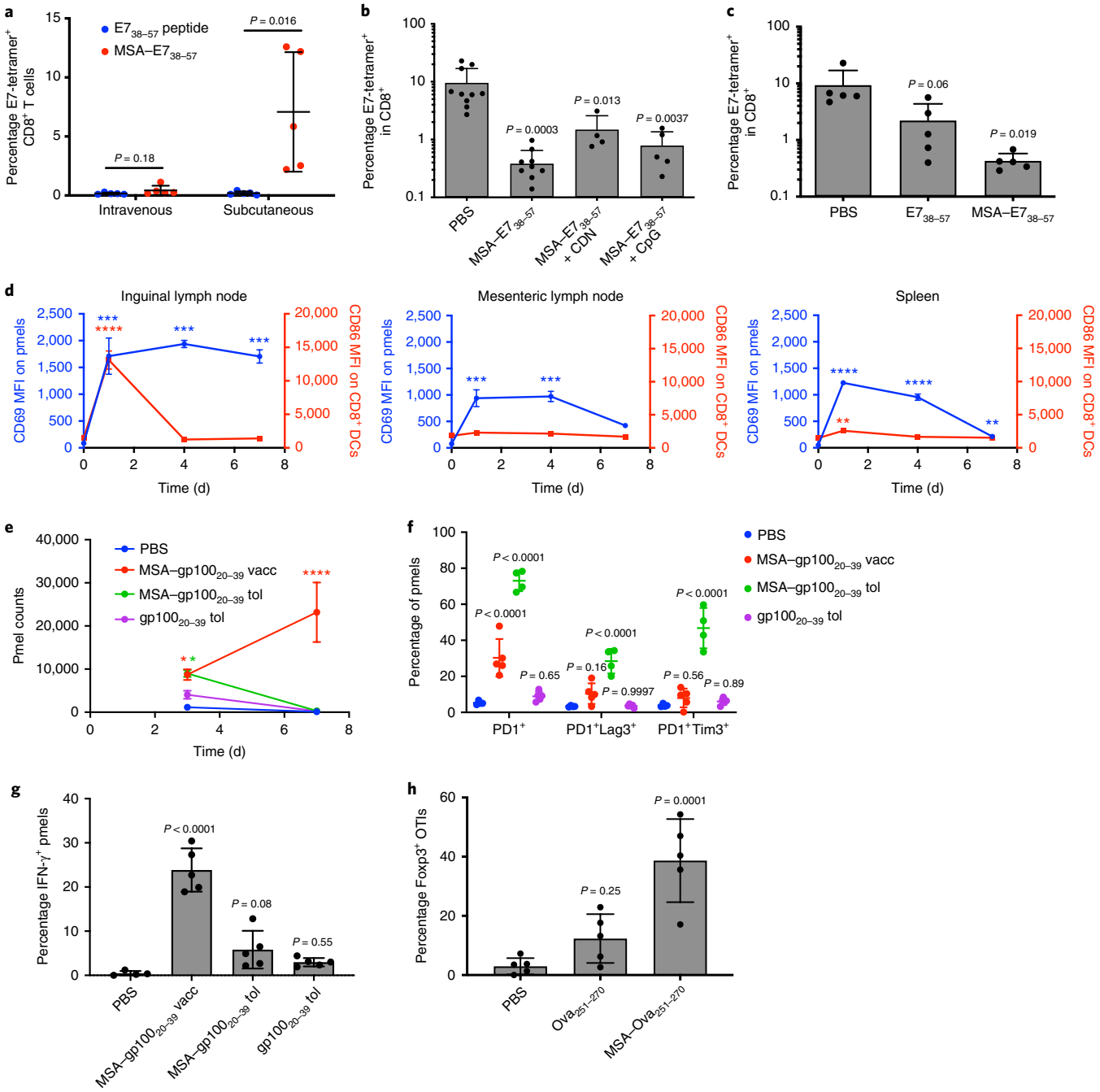

Fig. 3 | The systemic distribution of albumin fusions induces tolerance. a, Mice were subcutaneously or intravenously primed and boosted with either $E7_{38-57}$ or MSA-$E7_{38-57}$ and CDN. Tetramer-stain data of $CD8^+$ T cells 6 d after the boost are shown (mean ± s.d.; $n = 5$ mice per group). Data are representative of two independent experiments. **b**,**c**, Mice were intravenously administered the indicated vaccine and subcutaneously prime-boost challenged 2 weeks later with $E7_{38-57}$-fusion and CDN. Tetramer-stain data of $CD8^+$ T cells 6 d after the challenge boost are shown (mean ± s.d.; **b**, $n = 10$ for PBS, $n = 9$ for MSA-$E7_{38-57}$, $n = 4$ for MSA-$E7_{38-57}$ + CDN and $n = 5$ for MSA-$E7_{38-57}$ + CpG; **c**, $n = 5$ for all groups). **d**, Mice were subcutaneously administered MSA-$gp100_{20-39}$ APL with CDN. At 1, 4 and 7 d post-vaccination, 0.5×10^6 $CD8^+Thy1.1^+$ pmel cells were transferred into the mice. The indicated organs were excised 24 h after the cell transfer and the CD69 MFI was measured on $Thy1.1^+$ cells by flow cytometry. At the same time points post-vaccination, the indicated organs were excised and the CD86 MFI measured on $CD8^+$ DCs by flow cytometry (mean ± s.e.m.; $n = 3$ mice per group). $^{**}P < 0.01$, $^{***}P < 0.001$ and $^{****}P < 0.0001$. **e**–**g**, $CD8^+Thy1.1^+$ pmel cells (1×10^6) were transferred into WT mice. The indicated tolerizing vaccines were intravenously administered 24 h later without adjuvant (MSA-$gp100_{20-39}$ and $gp100_{20-39}$ tol), and an activating vaccine was administered subcutaneously with adjuvant (MSA-$gp100_{20-39}$ vacc; $n = 4$ mice for PBS and $n = 5$ for all other groups). **e**, $Thy1.1^+$ cell counts in the spleen 3 and 7 d after vaccination (mean ± s.e.m.). **f**, Frequency of expression of exhaustion-associated markers on $Thy1.1^+$ cells from inguinal lymph nodes on day 3 (mean ± s.d.). **g**, IFN-γ production by $Thy1.1^+$ cells from the inguinal lymph node on day 3 (mean ± s.d.). **h**, $CD8^+Thy1.1^+$ OT1 cells (1×10^6) were transferred into WT mice. The indicated tolerizing vaccines were intravenously administered 24 h later without adjuvant (mean ± s.d.; $n = 5$). The frequency of expression of Foxp3 on $Thy1.1^+$ cells from the inguinal lymph node on day 3 is shown. Statistical significance was calculated using a two-tailed Student's *t*-test between groups on the *x* axis with Holm–Sidak's multiple comparisons test (**a**), one-way ANOVA with Dunnett's multiple comparisons test versus the PBS group (**b**,**c**,**e**–**h**) or the day 0 time point for each measurement (**d**), and a two-way ANOVA with Dunnett's multiple comparisons test versus the PBS group (**f**).

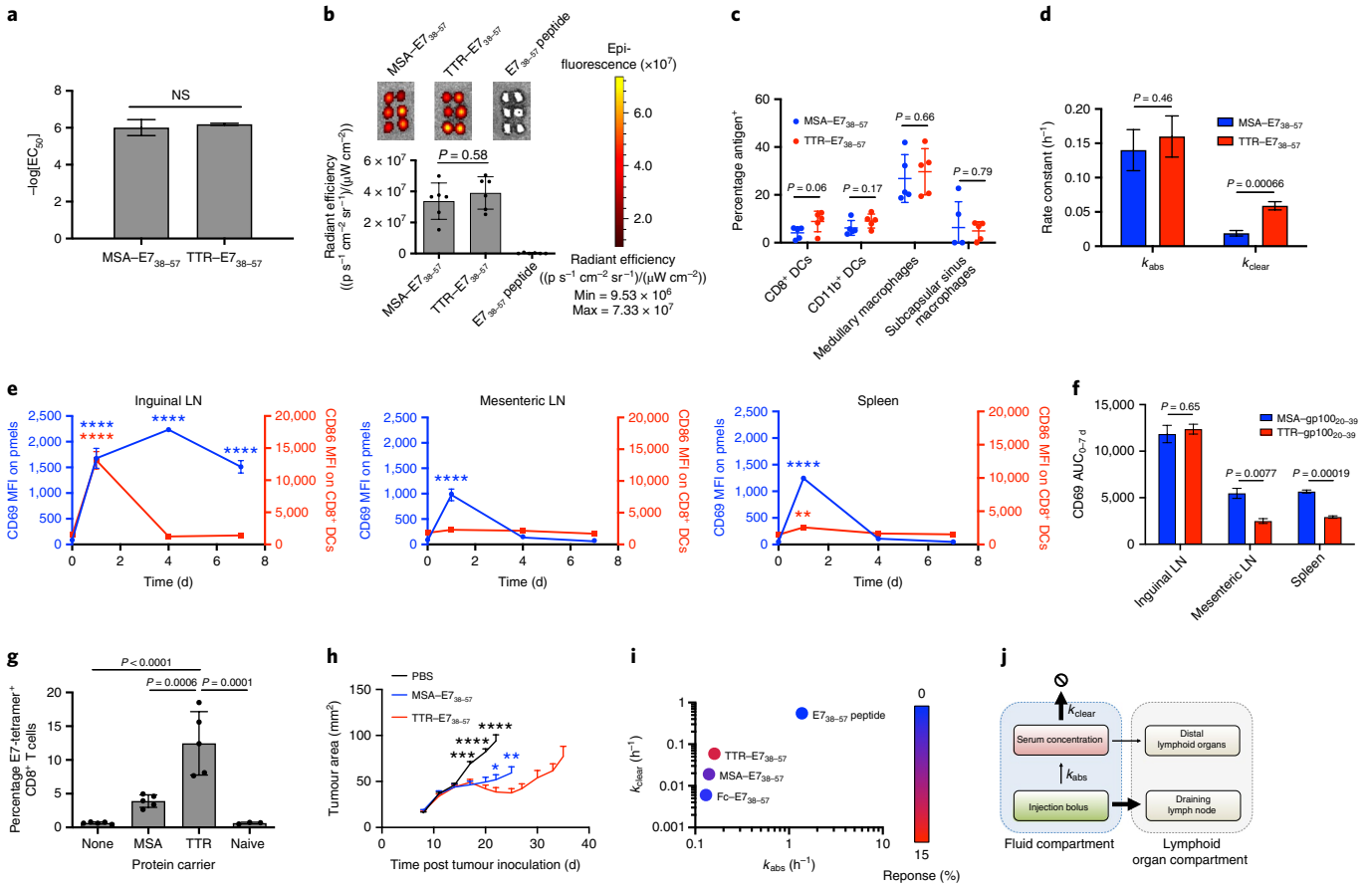

Fig. 4 | TTR fusions outperform MSA fusions due to a faster clearance rate. a, Half-maximum effective concentration (EC_{50}) values calculated from splenocyte restimulation studies with the indicated antigen ($n=3$). NS, not significant. **b**, Uptake of FITC-labelled antigen in the dLN, measured as in Fig. 1f (mean ± s.d.; $n=6$ lymph nodes per group). **c**, Alexa Fluor 488-labelled MSA-$E7_{38-57}$ or TTR-$E7_{38-57}$ were subcutaneously injected in mice. The inguinal lymph node was excised 24 h later and the Alexa Fluor 488 signal in APCs was assessed by flow cytometry (mean ± s.d.; $n=5$ mice per group). **d**, A nonlinear regression from pharmacokinetic studies was used to calculate the k_{abs} and k_{clear} values (fit data ± standard error). **e**, Pmel CD69 and CD8+ DC CD86 MFIs (mean ± s.e.m.; $n=3$ mice per group). **f**, Calculated AUC values from the CD69 MFI in Figs. 3d and 4e (calculated AUC ± standard error). **g**, Mice were subcutaneously primed and boosted with the indicated vaccine plus CDN. Tetramer-stain data of $CD8^+$ T cells 6 d after boost are shown (mean ± s.d.; $n=5$ mice per group). Data are representative of over five independent experiments. **h**, Mice were implanted with TC-1 tumour cells and immunized on days 8 and 15 with the indicated vaccine. The tumour growth curves of the indicated groups are shown (mean + s.e.m.). The curves for each group are plotted until the point where the first mouse was euthanized ($n=9$ mice per group). **i**, Mice were subcutaneously primed and boosted with the indicated vaccine plus CDN. Tetramer-stain data are indicated according to a colour code overlaid on a k_{abs} and k_{clear} scatterplot. **j**, Schematic of the pharmacokinetic parameters that maximize bioavailability in the inflamed dLN. **a**–**g**, Statistical significance was calculated using a two-tailed Student's *t*-test alone (**a**) or with a Holm–Sidak multiple comparisons test (**c**,**d**,**f**), a one-way ANOVA with Tukey's multiple comparisons test between all groups (**b**,**g**) or with Dunnett's multiple comparisons test against the day-zero time point for each measurement (**e**). **h**, Two-tailed Student's *t*-tests were performed at each measurement comparing against TTR-$E7_{38-57}$. **e**,**h**, $^*P<0.05$, $^{**}P<0.01$, $^{***}P<0.001$ and $^{****}P<0.0001$.

of regulatory T cells, $CD8^+$ T_{regs}, in tolerance and autoimmune disease[38–40]. In a similar study with transferred Thy1.1+ OTI cells and subsequent intravenous administration of PBS, $Ova_{251-270}$ peptide or MSA–$Ova_{251-270}$ without adjuvant, the frequency of $Foxp3^+$ Thy1.1+ cells was elevated in the inguinal lymph node on day 3 most significantly in the mice that received MSA fusion without adjuvant. Collectively, we conclude that the delivery of albumin fusions in the absence of adjuvant facilitates tolerization by depleting and/or exhausting antigen-specific T cells and by stimulating the development of previously characterized $Foxp3^+CD8^+$ T_{regs}.

Increasing k_{clear} can further improve immunogenicity. The tolerizing impact of persistent systemically distributed protein compelled us to search for an alternative protein carrier that preserved the low k_{abs} of albumin while exhibiting a more rapid systemic k_{clear} constant to decrease systemic antigen exposure while maintaining local lymph node accumulation. We identified transthyretin (TTR), a tetrameric endogenous hormone-trafficking serum protein of approximately 60 kDa, as a promising candidate protein carrier because it has a similar molecular weight to albumin but a significantly shorter systemic half-life ($t_{1/2}$ of about 2 d for TTR[41] versus $t_{1/2}$ of about 3 weeks for albumin[42]). Although TTR amyloidosis diseases demonstrate its propensity to form aggregates in solution, these conditions typically result from mutant rather than wild-type (WT) TTR, and fibril formation is driven by acidic rather than physiologic conditions[43]. After expression, we found TTR–$E7_{38-57}$ to be stably monomeric without evidence of fibril formation, similar to MSA–$E7_{38-57}$ (Supplementary Fig. 1b).

We next confirmed TTR to be similar to MSA in all characteristics except k_{clear}. The $E7_{38-57}$ peptide was processed and presented by either fusion protein with similar potency during ex vivo splenocyte restimulation (Fig. 4a) and, similar to MSA–$E7_{38-57}$, TTR–$E7_{38-57}$ was

Table 1 | Overview of the pharmacokinetic determinants of vaccine immunogenicity

	1. Size exclusion from systemic absorption			2. Proteolytic stability	3. Avoidance of distal priming	Immunogenicity
Antigen construct	**MW (kDa)**	**Radius (nm)**	**k_{abs} (h^{-1}; fit data ± standard error)**	**Serum-treated antigen recall response relative to fresh (%)**	**k_{clear} (h^{-1}; fit data ± standard error)**	**Vaccine response (percentage of $CD8^+$ T cells; mean ± s.d.)**
$E7_{38-57}$ peptide	2.2	—	1.37 ± 0.40	21.5	0.55 ± 0.11	0.12 ± 0.07
Fc–$E7_{38-57}$	57.8	3.4	0.13 ± 0.02	59.3	0.006 ± 0.002	1.94 ± 0.69
MSA–$E7_{38-57}$	69.4	3.3	0.14 ± 0.03	114	0.019 ± 0.004	5.94 ± 1.38
TTR–$E7_{38-57}$	68.5	3.5	0.16 ± 0.03	61.0	0.059 ± 0.006	12.45 ± 4.70

stable in serum (Supplementary Fig. 10a). Following subcutaneous administration, FITC–TTR–$E7_{38-57}$ accumulated in the inguinal dLN at levels equivalent to FITC–MSA–$E7_{38-57}$ (Fig. 4b) and was taken up by APCs similarly (Fig. 4c).

In contrast, MSA–$E7_{38-57}$ and TTR–$E7_{38-57}$ had distinct pharmacokinetic properties following subcutaneous administration (Fig. 1c versus Supplementary Fig. 10b). Although the k_{abs} was similar between MSA–$E7_{38-57}$ and TTR–$E7_{38-57}$ ($0.14 \pm 0.03\,h^{-1}$ and $0.16 \pm 0.03\,h^{-1}$, respectively), the k_{clear} was over threefold faster for TTR–$E7_{38-57}$ than MSA–$E7_{38-57}$ ($0.019 \pm 0.004\,h^{-1}$ versus $0.059 \pm 0.006\,h^{-1}$; Fig. 4d). When reporter pmels were used to assess T-cell priming kinetics following TTR–$gp100_{20-39}$ immunization, we found that the faster $k_{clear}$of TTR led to more transient priming in distal, uninflamed lymphoid organs than observed with MSA fusions, with CD69 expression detected only in the mesenteric lymph node and spleen at 1 day post-immunization with TTR–$gp100_{20-39}$ (Fig. 4e). Although the area under the curve (AUC) of the mean fluorescent intensity (MFI) of CD69 at 1 week was similar between MSA and TTR fusions in the draining inguinal lymph nodes, the AUCs in the mesenteric lymph nodes and spleen were significantly reduced for TTR fusions (Fig. 4f). Correlating with these findings, subcutaneous immunization with TTR–$E7_{38-57}$ elicited a $CD8^+$ T-cell response that was 3.7-fold higher than MSA–$E7_{38-57}$ when dosed with equimolar E7 antigen (Fig. 4g), and no immunophenotypic differences in terms of memory precursor populations or expression of T-bet, granzyme B, KLRG1 and CD127 could be detected (Supplementary Fig. 11). TC-1-bearing mice treated with TTR–$E7_{38-57}$ exhibited greater tumour growth inhibition than mice treated with MSA-$E7_{38-57}$ (Fig. 4h). No antibody responses against TTR were detectable (Supplementary Fig. 6c,d).

To further confirm the effect of k_{clear} on the immunogenicity of fusion protein vaccines, we fused and characterized the Fc portion of an IgG2c antibody to $E7_{38-57}$ (Fc–$E7_{38-57}$; Supplementary Fig. 1c), generating a fusion construct with a k_{clear} value 10× slower than TTR–$E7_{38-57}$ and 3× lower than MSA–$E7_{38-57}$ ($k_{clear} = 0.006 \pm 0.002\,h^{-1}$; Supplementary Fig. 10d). Following prime and boost, Fc–$E7_{38-57}$ and CDN vaccination primed a 1.7% $E7_{49-57}$-specific $CD8^+$ T-cell response, a 24-fold boost in immunogenicity compared with peptide vaccination, which was nonetheless weaker than the responses to MSA–$E7_{38-57}$ and TTR–$E7_{38-57}$ (Supplementary Fig. 12). Although IgG2c is an activating Fc isotype that binds to Fc receptors, mutations that reduced binding to FcγRs and FcRn did not affect the immunogenicity of Fc–$E7_{38-57}$ (Supplementary Fig. 12). Overall, the efficacies of the different vaccines (TTR–$E7_{38-57}$ > MSA–$E7_{38-57}$ > Fc–$E7_{38-57}$ >> $E7_{38-57}$ peptide; Fig. 4i) suggest that although lowering k_{abs} is essential to generate vaccine responses over the background, increasing k_{clear} can further boost potency (Fig. 4j). Collectively, we conclude that size exclusion from systemic absorption, proteolytic stability and avoidance of antigen accumulation in uninflamed lymphoid organs all contribute to the immunogenicity of protein vaccines, which can be tuned and optimized by the judicious selection of protein fusion partner (Table 1).

TTR as a delivery vehicle in tumour immunotherapy. We next explored the generalizability of TTR delivery in the context of other tumour-associated antigens. As measured by the frequency of IFN-γ^+CD8^+ T cells in peripheral blood, TTR–antigen fusion vaccines outperformed MSA–antigen vaccines by fourfold for $Trp1_{1455-1463}$ and twofold for $gp100_{20-39}$ APL; while TTR–$CEA_{567-584}$ generated IFN-γ^+ responses equivalent to MSA–$CEA_{567-584}$, polyfunctional IFN-γ^+TNF-α^+ responses were enhanced over background only in the case of TTR–$CEA_{567-584}$ (Fig. 5a).

As a tetramer, TTR also provides the opportunity to develop constructs with higher valencies, which provide manufacturing advantages. For example, TTR fusions carrying two copies of the $E7_{38-57}$ epitope per subunit (eight copies per tetramer) reduced the volume of production cell culture required for vaccination by 4.7-fold compared with MSA–$E7_{38-57}$ (Supplementary Fig. 13a), with no corresponding loss in immunogenicity (Supplementary Fig. 13b,c). We reasoned that if the fusion of multiple copies of epitopes to TTR preserved immunogenicity, then the protein carrier could be designed to deliver multiple antigens simultaneously. Although the co-delivery of antigens on a single molecule can simplify commercial translation, it runs the risk of biasing responses towards the most immunogenic antigen in the construct. To assess this risk, we administered the TTR–$gp100_{20-39}$ and TTR–$Trp1_{1455-1463}$ vaccines, separately or together, and compared immune responses against TTR fused to $gp100_{20-39}$ and $Trp1_{1455-1463}$ simultaneously in either orientation (Fig. 5b). TTR carriers delivering both antigens together elicited T-cell responses that did not statistically differ from the individual or mixed antigens, and we observed no dependence on antigen order in the fusion constructs (Fig. 5b).

We assessed the therapeutic responses to Trp1 and gp100 vaccination in the aggressive B16F10 melanoma model to test the therapeutic efficacy of this strategy. Subcutaneous B16F10 tumours were vaccinated with free Trp1 and gp100 peptides or TTR–Trp1–gp100 fusions every 6 d with or without anti-PD1 combination therapy (Fig. 6a). Six days after the first boost, strong antigen-specific IFN-γ^+ T-cell responses (mean > 25%) were only generated in groups vaccinated with TTR–Trp1–gp100 (Fig. 6b). As a result, mice treated with TTR–Trp1–gp100 had significantly slower tumour outgrowth than mice treated with the Trp1 and gp100 peptides (Fig. 6c). Anti-PD-1 therapy had no efficacy as a monotherapy but elicited substantially enhanced antitumour efficacy when administered together with the TTR-fusion vaccine (Fig. 6d). Statistically significant improvements in overall survival relative to the PBS controls were observed only in mice receiving TTR-fusion vaccines (Fig. 6e).

Shared neoantigens, or human leukocyte antigen (HLA)-displayed peptides derived from mutant oncogenes, are also emerging as promising targets of vaccination. We tested two

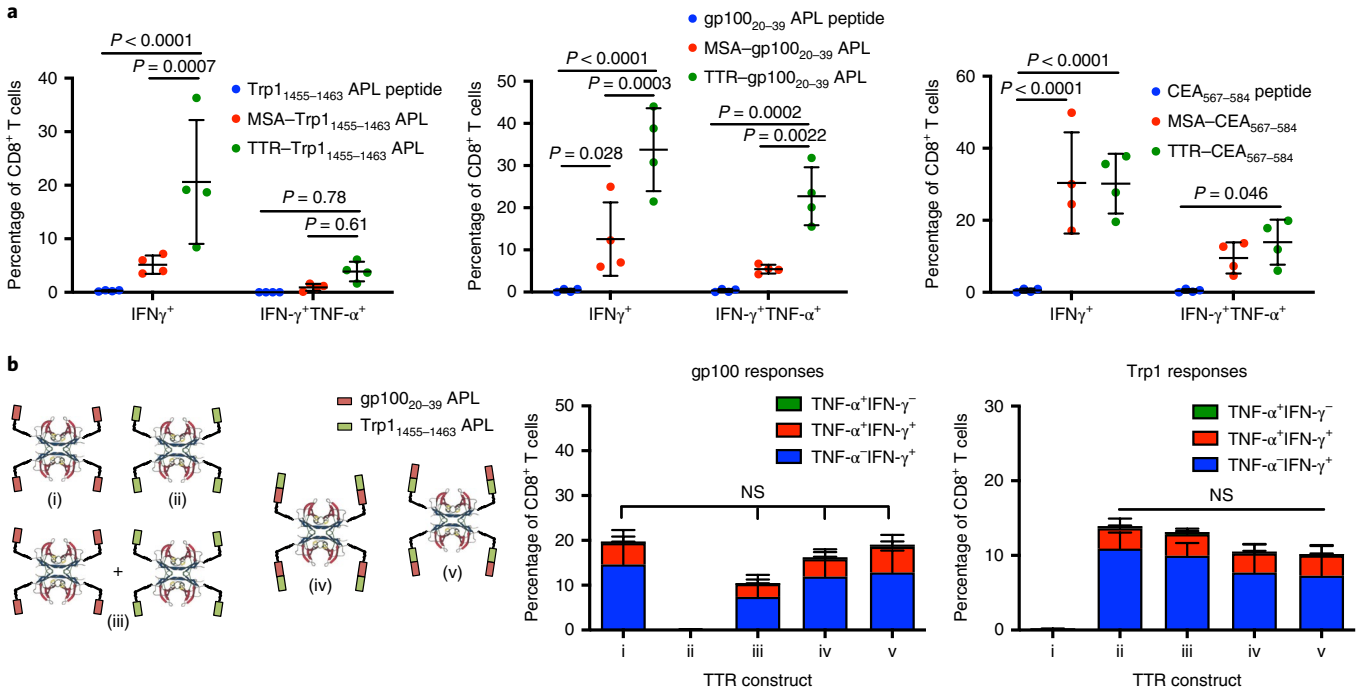

Fig. 5 | TTR-antigen fusion vaccines. a, Mice were subcutaneously primed and boosted with the indicated antigens in peptide, MSA-fusion or TTR-fusion form along with CDN and then assessed by ICS (mean ± s.d.; $n = 4$ mice per group). **b**, Schematic of the TTR constructs used to test the Trp1 and gp100 orientation during co-delivery (left). Mice were vaccinated with constructs along with CDN. ICS data 6 d after boost (right; mean ± s.d.; $n = 5$ mice per group). Statistical significance was calculated using a two-way ANOVA with Tukey's multiple comparisons test (**a**) or one-way ANOVA with Tukey's multiple comparisons test (**b**).

shared neoantigens with TTR fusions: Kras G12D, commonly mutated in pancreatic cancer[44,45], and H3.3 K27M, a driver mutation in paediatric gliomas[46–48]. HLA-A11- and HLA-A2-displayed epitopes have recently been identified for Kras G12D and H3.3 K27M mutations, respectively[49,50]. HLA-A11 and HLA-A2 transgenic mice were prime–boosted with the $Kras_{2\text{-}21,G12D}$ and $H3.3_{21\text{-}40,K27M}$ peptides or TTR-fusion vaccines, followed by an ELISpot read-out. Antigen-specific cellular immunity above background was observed only with TTR fusion (Fig. 6f,g). Together, these data demonstrate the utility of TTR-mediated delivery for viral antigens (E7), tumour-associated antigens (Trp1 and gp100), oncofetal antigens (CEA) and shared neoantigens ($Kras_{G12D}$ and $H3.3_{K27M}$).

Discussion

A major factor limiting the potency of peptide vaccines is their poor transport to lymph nodes following injection[14]. This transport limitation has spurred the development of a broad set of delivery platforms to improve antigen delivery to lymph nodes; these strategies have mostly entailed nanoparticulate formulation and/or chemical modification of synthetically produced peptide vaccines[14,18,19,51–53]. Here we altered the biodistribution of peptides by fusing these antigens to protein-based delivery vehicles to develop a fully recombinant protein solution. We demonstrated that protein–epitope fusions are strong candidate vehicles for off-the-shelf vaccination against targets such as viral antigens, tumour-associated antigens, oncofetal antigens and shared neoantigens.

Peptides are routinely conjugated to immunogenic protein carriers, such as keyhole limpet haemocyanin (KLH), to increase B-cell receptor crosslinking and co-deliver antigen with CD4+ T-cell epitopes, boosting humoral immunity[54]. However, T-cell responses are exclusively detected against KLH and not against the antigen of interest[55]; and the impacts of KLH on biodistribution have been understudied. Here we utilized minimally immunogenic protein carriers to direct cellular responses against fused epitope payloads and we tuned immunogenicity by the modulation of pharmacokinetics. While this work focused on the delivery of CD8+ T-cell epitopes, future efforts should be made to understand how the protein-fusion strategy influences CD4+ T-cell responses against long peptide antigens.

Analysis of the biodistribution behaviour of several protein carrier–epitope fusion vaccines revealed principles for optimizing vaccine immunogenicity via pharmacokinetic tuning. We found that maximizing the bioavailability in the dLN but reducing uptake in distal lymphoid organs ensures that the antigen is presented at the right site at the right time. Two rate constants controlling local lymphatic versus systemic distribution, k_{abs} and k_{clear}, predictably influenced antigen biodistribution and thus had a dominant effect on vaccine immunogenicity. When these two rate constants are appropriately selected, as in the case of TTR, vaccine responses can be significantly potentiated in both magnitude and functionality, delaying the growth of checkpoint-refractory tumours in mice.

In particular, appropriately bulky protein carriers reduced the k_{abs} sufficiently to reduce systemic absorption following subcutaneous injection, thereby improving lymphatic uptake and subsequent accumulation in the dLN. However, while dLN bioavailability is a prerequisite to potent vaccination, increasing the k_{clear} can further improve immunogenicity by limiting antigen accumulation in distal lymphoid organs that have not received adjuvant stimulation. Adjuvants are typically designed to avoid systemic dissemination to prevent unacceptable toxicities[14,56,57] and result in inflammation at only the local dLNs, as observed here with CDNs. However, antigens with a low k_{clear} will systemically distribute into uninflamed distal lymphoid organs, leading to dysfunctional priming of T cells at these sites. This principle is supported by the hierarchy of immunogenicity we observed with TTR, MSA and Fc fusions. Recognition of this phenomenon

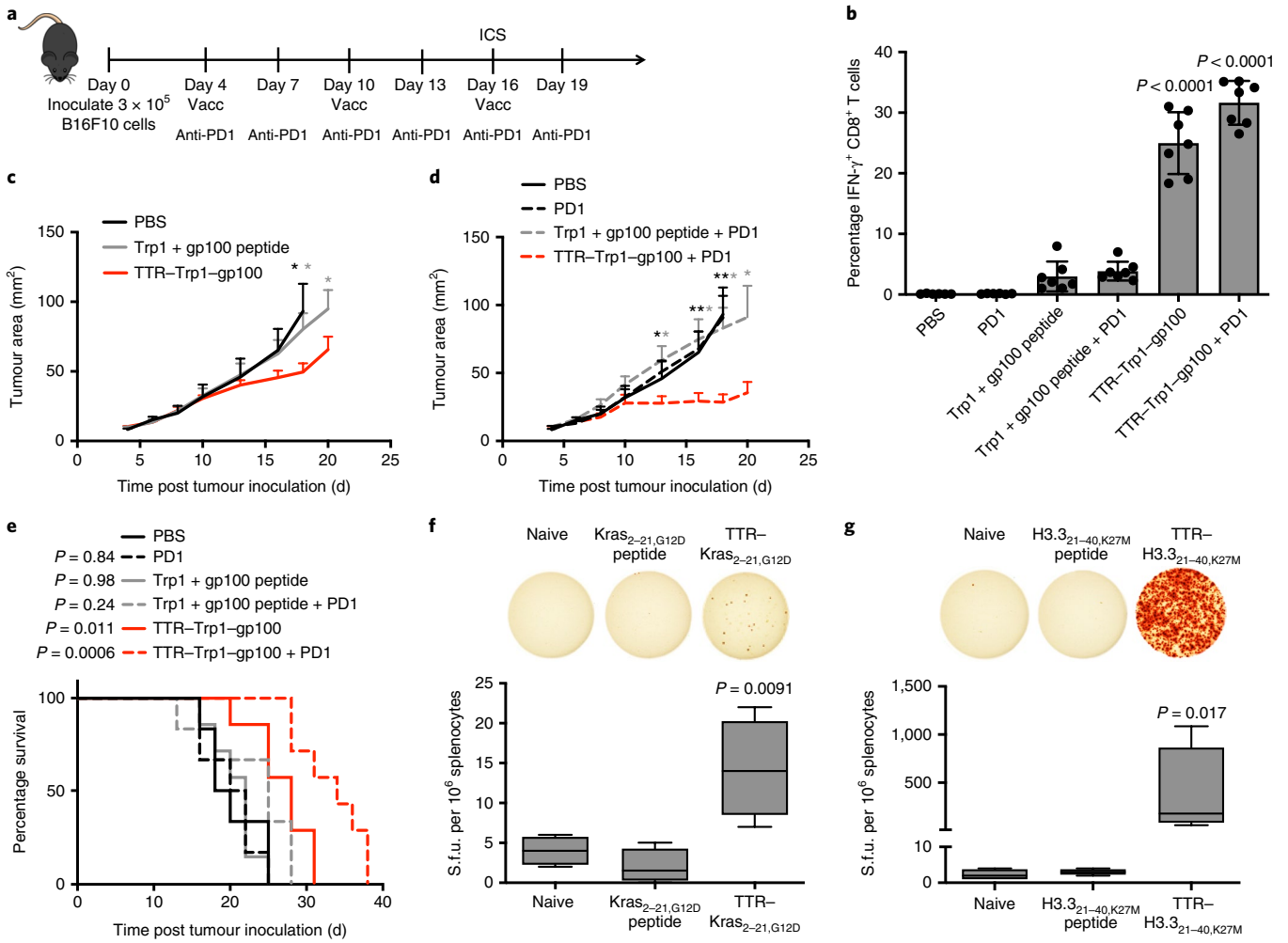

Fig. 6 | TTR-antigen fusions in cancer immunotherapy. a, Schematic of the B16F10 tumour immunotherapy study timeline used to generate panels **b–e** ($n = 6$ mice for the PBS and Trp1 + gp100 peptide + PD1 groups, and $n = 7$ mice for all other groups). Vacc, vaccination. **b**, ICS data collected from PBMCs on day 16 of the B16F10 study. The pooled Trp1 and gp100 responses of the $CD8^+$ T cells in blood are shown (mean ± s.d.). **c**,**d**, Tumour growth curves of the indicated groups (mean + s.e.m.). The curves for each group are plotted until the point where the first mouse was euthanized. **e**, Survival curves. **f**,**g**, Vaccines targeting the indicated neoantigens were administered with prime-boost in HLA-A11 (**f**) and HLA-A2 (**g**) transgenic mice, followed by an ELISpot (top) read-out with splenocytes stimulated with overlapping peptides containing neoantigen ($n = 4$ mice per group). Boxplot representations of the spot counts, with the median, interquartile range, and minimum and maximum identifiers are shown (bottom); s.f.u., spot-forming units. **b**–**g**, Statistical significance was calculated using a two-way ANOVA with one-way ANOVA with Dunnett's multiple comparisons test versus the PBS (**b**) or naive (**f**) groups, one-tailed Student's *t*-test at each measurement versus the TTR-Trp1-gp100 (**c**) or TTR-Trp1-gp100 + PD1 (**d**) groups, two-tailed log-rank (Mantel–Cox) test versus PBS (**e**) or Kruskal–Wallis with Dunn's multiple comparisons test versus the naive group (**g**). **c**,**d**, $^*P < 0.05$ and $^{**}P < 0.01$.

has practical implications in vaccine engineering. For example, the observation of priming in distal nodes was noted in early antibody-mediated DEC-205-targeted immunization studies, necessitating the co-administration of a systemic adjuvant, which would probably be too toxic for clinical translation[21]. Simply matching the pharmacokinetics of the antigen and adjuvant such that they similarly distribute in vivo may be a facile alternative to manufacturing antigen–adjuvant conjugates or co-encapsulations. There is opportunity for further engineering in this regard, as even TTR fusions lead to antigen presentation in the dLN that outlasts inflammatory cues. The use of appropriately persistent protein–antigen fusions to treat autoimmunity should also be further explored.

Protein–epitope fusions also avoid a number of manufacturing and scale-up issues commonly associated with nanoparticulate formulations. Mass production of protein biologics is a well-developed art, and recombinant proteins can be manufactured using good manufacturing practice processes at scale to high purity. Albumin has been used for decades to help solubilize challenging cargo; although TTR is a less commonly utilized carrier, it can also be homogeneously produced, and as a tetramer its manufacturing efficiency is improved several-fold.

The protein–epitope fusion approach also has a potential application in nucleic acid vaccination—a cheaper, rapidly deployable modality. Intramuscular transfection with plasmid DNA and/or messenger RNA are both commonly studied vaccination strategies[58–60]. Encoding protein–epitope fusions in these systems could allow for the expression of the antigen payload fused to a protein delivery vehicle to shepherd antigen from the site of secretion to the dLN. Non-encodable, particulate or conjugate-based delivery systems are not amenable to such an approach.

Notably, the pharmacokinetic determinants of immunogenicity described here can be elucidated with a low number of simple, rapid and cost-effective experiments. Data on the k_{abs} and k_{clear} can be

assessed with a single pharmacokinetic study and proteolytic stability can be reliably measured by performing restimulation assays ex vivo on vaccinated or transgenic splenoctyes with fresh or serum-treated antigen. We propose that these two assays can be used to rapidly screen and optimize future protein-carrier strategies and improve future efforts to prime functional antitumour immunity.

Methods

Mice. B6 (C57BL/6NTac) and HLA-A11 (B6-Tg(HLA-A*1101/H2-Kb)A11.01) mice were purchased from Taconic. *Batf3*$^{-/-}$ (B6.129S(C)-Batf3^{tm1Kmm}/J), pmel Thy1.1^{+} (B6.Cg-Thy1a/Cy Tg(TcraTcrb)8Rest/J) and HLA-A2 (C57BL/6-Mcph1Tg(HLA-A2.1)1Enge/J) mice were purchased from Jackson Laboratory. OTI (C57BL/6-Tg(TcraTcrb)1100Mjb/J) and Thy1.1 (B6.PL-Thy1a/CyJ) mice were purchased from Jackson Laboratory and crossed to generate an OTI Thy1.1^{+} colony. All animal work was conducted under the approval of the Massachusetts Institute of Technology Division of Comparative Medicine in accordance with federal, state and local guidelines. A summary of the mouse strains used in each study is outlined in Supplementary Table 1.

Cells. HEK cells (FreeStyle 293-F) were purchased from Thermo Fisher Scientific. The TC-1 cell line, an HPV E6- and E7-expressing line derived from C57BL/6 lung epithelia, was kindly provided by T. C. Wu (Johns Hopkins University). The B16F10 cell line, a mouse model of melanoma, was purchased from American Type Culture Collection. HEK cells were cultured in FreeStyle 293 expression medium (Thermo Fisher Scientific) and passaged every 2 d to a density of 3×10^5 cells ml^{-1}. TC-1 cells were cultured in RPMI-1640 medium (GE Healthcare Life Sciences) supplemented with 10% fetal bovine serum (FBS), 100 units ml^{-1} penicillin, 100 µg ml^{-1} streptomycin and 4 mM L-alanyl-L-glutamine. B16F10 cells were cultured in DMEM medium (GE Healthcare Life Sciences) supplemented with 10% FBS, 100 units ml^{-1} penicillin, 100 µg ml^{-1} streptomycin and 4 mM L-alanyl-L-glutamine. Both tumour cells were passaged 1:10 every 2 d. All cells were cultured at 37 °C and 5% CO_2. All cells were tested regularly for mycoplasma contamination and rodent pathogens, and none tested positive at any point. A summary of the cell lines used for each tumour study is outlined in Supplementary Table 1.

Protein expression and purification. Codon-optimized genes encoding the desired proteins were cloned into gWiz expression vectors (Genlantis) using the In-Fusion HD cloning kit (Clontech), prepared endotoxin free (Macherey-Nagel) and incubated with Opti-Pro (Thermo Fisher Scientific) and polyethylenimine (PEI 25K; Polysciences) before drop-wise addition to the HEK cell culture at 1×10^6 cells ml^{-1}. DNA (1 mg) was mixed with 40 ml Opti-Pro and 2 mg polyethylenimine per 1 l of cell culture. One week after transfection, the cell culture was spun down in endotoxin-free centrifuge tubes at 15,000*g* for 30 min, and the supernatant was filtered, pH neutralized by the addition of 10×PBS and run through TALON metal affinity resin (Clontech) by gravity flow as per the manufacturer's instructions. Fc–E7$_{38-57}$ and its variants were prepared as heterodimers with one copy of E7$_{38-57}$ per Fc dimer by co-transfecting gWiz–Fc–His$_6$–E7$_{38-57}$ and gWiz–Fc–FLAG (0.5 mg of each plasmid per 1 l cell culture). Purification proceeded as above, but the eluate from the TALON resin was subsequently run through an anti-DYKDDDDK G1 affinity resin kit (Genscript) as per the manufacturer's instructions to ensure purification of the heterodimer. In addition to WT Fc fusions, a pair of mutations (G236R/L328R) were introduced to knock out binding to FcγRs[61]. Following purification, the proteins were buffer exchanged into PBS with 30-kDa molecular-weight cutoff Amicon Ultra-15 centrifugal filters (Millipore), filtered using Spin-X centrifuge tube filters (Corning) or 0.2-µm syringe filters (VWR), flash-frozen in aliquots with liquid nitrogen and then stored at −80 °C. After thawing, the proteins were stored at 4 °C in sterile conditions and used within one month. The protein sequences are outlined in Supplementary Table 2.

Protein characterization. The protein and dextran hydrodynamic radii were assessed by dynamic light scattering (DynaPro NanoStar), purity analysed by size-exclusion chromatography (Superdex 200 Increase) and the endotoxin levels were measured using a chromogenic LAL assay (Lonza). A maximum of 5 EU kg^{-1}, where EU indicates endotoxic units, or 0.1 EU per mouse was accepted for all injected proteins.

Pharmacokinetic studies. 5-FAM–E7$_{38-57}$ was purchased from Genscript and recombinantly expressed proteins (MSA–E7$_{38-57}$, TTR–E7$_{38-57}$ and Fc–E7$_{38-57}$) were labelled with NHS-5/6-FAM (Thermo Fisher Scientific) as per the manufacturer's instructions. Following protein conjugation, the concentration of the labelled protein was calculated using A_{493}. Mice were subcutaneously or intravenously vaccinated with 1 nmol labelled peptide or protein. At the indicated time points, <10 µl blood was collected from a tail snip into heparin-coated microhaematocrit capillary tubes (VWR). The capillaries were parafilmed and stored upright in the dark at 4 °C overnight to separate the serum from cellular components. The serum in capillaries was measured on a Typhoon Trio variable mode imager (526 SP filter and 532 nm laser) against a standard curve of analytes prepared in PBS and added directly into capillaries. FIJI image analysis software was used to calculate the serum concentrations of the analyte. Intravenous curves were fit to $C = C_0 e^{-k_{clear}\times t}$ and subcutaneous curves were fit to $C = F\times C_0\times k_{abs} \div (k_{abs} - k_{clear})\times (e^{-k_{clear}\times t} - e^{-k_{abs}\times t})$, where C is the serum concentration of vaccine over time, C_0 is the initial serum concentration and F is the systemic absorbance. C_0 and k_{clear} were fixed by intravenous fit. The curves were fit using nonlinear regression on GraphPad Prism software.

Vaccinations. All activating vaccinations were performed by subcutaneous prime at the tail base on day 0, boost on day 14 and read-out on day 20, except for the intravenous vaccination in Fig. 3a. All studies utilized 25 µg cyclic di-GMP (InvivoGen) as the adjuvant unless otherwise specified—in Fig. 2c, 1 nmol ODN1826 (CpG; InvivoGen), 50 µg poly(I:C) HMW (Invivogen) and 1 nmol lipo-CpG[14] were used instead as alternative adjuvants; 50 µg cyclic di-GMP was used in TC-1 tumour-bearing animals and 1 nmol lipo-CpG was used as the adjuvant in the B16F10 tumour study. Antigen dosing (expressed as peptide equivalence) was as follows: 3 µg for all E7$_{38-57}$ studies in non-tumour-bearing mice; 10 µg E7$_{38-57}$ in Fig. 2e; 5 µg E7$_{38-57}$ in Fig. 4h; 2.5 µg Trp1$_{1455-1463}$ APL, and 5 µg gp100$_{20-39}$ APL and CEA$_{567-584}$ in Figs. 2e and 5a, respectively; 3 µg gp100$_{20-39}$ APL or Ova$_{257-265}$ in pmel or OTI adoptive-transfer studies, respectively; for bivalent forms of TTR–Trp1–gp100, 2.5 nmol was used in non-tumour-bearing mice and 4 nmol in tumour-bearing mice; and 10 µg Kras$_{2-21,G12D}$ and H3.3$_{21-40,K27M}$. For tolerizing vaccinations (Fig. 3b,c), PBS, 3 µg peptide equivalence E7$_{38-57}$ or MSA–E7$_{38-57}$ with or without adjuvant (25 µg cyclic di-GMP or 1 nmol lipo-CpG) was intravenously administered 14 d before subcutaneous prime–boost with TTR–E7$_{38-57}$ plus cyclic di-GMP as described above. In all cases, the vaccine responses were measured by tetramer stain, ICS (see the 'Flow cytometry' section) or by mouse IFN-γ ELISpot (BD Biosciences) as per the manufacturer's instructions, where 1×10^6 splenocytes were plated per well and stimulated with overlapping peptides (Kras$_{2-21,G12D}$ or H3.3$_{21-40,K27M}$) for 24 h.

Flow cytometry. Antibodies against CD16/32 (Fc block, clone 93), CD8α (53-6.7), TNF-α (MP6-XT22), IFN-γ (XMG1.2), CD3 (17a2), B220 (RA3-6B2), CD11b (M1/70), CD11c (N418), F4/80 (BM8), CD69 (H1.2F3), CD86 (GL-1), PD1 (29F.1A12), Lag3 (C9B7W) and Tim3 (RMT3-23) were purchased from BioLegend. Cell viability was assessed using DAPI (Sigma) for tetramer stains and LIVE/DEAD fixable aqua dead cell stain (Thermo Fisher Scientific) for all other studies.

Tetramer staining. The E7 tetramer (iTAg Tetramer/PE - H-2D^b HPV 16 E7) was purchased from MBL; during tetramer staining, PBMCs were Fc blocked and stained with the tetramer for 15 min before the addition of anti-CD8α antibody, and the cells were incubated with all antibodies for another 30 min. All labelling was performed in PBS + 0.1% BSA.

Ex vivo stimulation studies. Intracellular cytokine staining to assess the magnitude of the T-cell responses was performed as previously reported[62]. Briefly, PBMCs were restimulated in RPMI-1640 medium containing 10% FBS at 37 °C with optimal WT peptide at 10 µg ml^{-1} (Trp1$_{1455-1463}$, gp100$_{25-33}$ and CEA$_{572-579}$) for 2 h, followed by the addition of brefeldin A (Thermo Fisher Scientific) for another 4 h before staining. In the B16F10 study, restimulation was performed with 10 µg ml^{-1} of both Trp1$_{1455-1463}$ and gp100$_{25-33}$. When ICS was used to assess stability/immunogenicity instead of a vaccine read-out, whole protein or long peptide antigen was used for stimulation (see the 'Antigenic-stability analysis' section) and cells were restimulated for 18 h, followed by the addition of brefeldin A for another 6 h before staining. In all cases, surface staining was performed first (Fc block and anti-CD8α) in PBS containing 0.1% BSA, followed by fixation and permeabilization using a BD cytofix/cytoperm fixation/permeabilization kit as per the manufacturer's instructions and intracellular staining (anti-IFN-γ and/or anti-TNF-α) in perm/wash buffer. To assess the immunogenicity of protein or peptide antigens at stimulating OTI cells, pooled ACK-lysed splenocytes from OTI mice were cultured in RPMI-1640 containing 10% FBS and varying concentrations of SIINFEKL-containing antigen for 24 h; after culture, the cells were surface labelled with anti-CD8α and anti-CD69.

Organ processing. In studies where T cells from lymph nodes were assessed by flow cytometry (Figs. 3d–h and 4e), the lymph nodes were excised, mashed through 74-µm Netwell inserts (Corning) and washed with PBS containing 0.1% BSA before antibody labelling. In studies where dendritic cells and/or other APCs were assessed by flow cytometry (Figs. 3d, 4c,e and Supplementary Fig. 8e), the lymph nodes were excised, digested in RPMI-1640 medium containing 0.8 mg ml^{-1} collagenase/disapse (Sigma) and 0.1 mg ml^{-1} DNase I (Sigma), mashed through 74-µm Netwell inserts and washed with PBS containing 0.1% BSA before antibody staining. In all cases, the spleens were excised and mashed through 70-µm filters (Corning), lysed in ACK buffer and washed in PBS containing 0.1% BSA before antibody staining. To assess CD86 expression on DCs post-immunization, mice were subcutaneously injected with 25 µg cyclic di-GMP (InvivoGen), and the spleen and inguinal and mesenteric lymph nodes were excised and processed 1,

4 or 7 d later. Cells were analysed using the BD FACSCanto and BD FACS LSR Fortessa systems, and data were analysed using FlowJo.

Antigenic-stability analysis. *Ex vivo stimulation method.* Mice were primed with $E7_{38-57}$ fusion protein mixed with CDNs 20 d in advance, boosted 6 d in advance and strong peripheral antigen-specific $CD8^+$ T-cell responses were confirmed on day 0. On the day of the experiment, the spleens from the vaccinated animals were excised, mashed through 70-µm filters (Corning), lysed in ACK buffer, pooled and plated in 96-well v-bottom plates (one spleen per 30 wells). Before ex vivo stimulation (24 h), serum from naive mice was freshly collected in collection tubes with Z-Gel to remove clotting factors (Sarstedt) and used to prepare RPMI-1640 medium containing 10% mouse serum media. Antigen solutions (4 µM) were prepared in RPMI-1640 + 10% mouse serum and incubated at 37 °C. After an incubation of 24 h, fresh antigen was similarly prepared at 4 µM in RPMI-1640 + 10% mouse serum and both solutions were immediately diluted to a 25 nM solution with RPMI-1640 + 10% FBS and used to re-stimulate the aforementioned splenocytes from the vaccinated animals. The IFN-γ^+CD8^+ T-cell responses were measured through ICS.

ELISA method. Fresh mouse plasma was prepared by bleeding directly into microcentrifuge tubes and spin removal of cellular matter, maintaining the functional complement and clotting factor components. FLAG–$E7_{38-57}$–His_6 peptide and MSA–FLAG–$E7_{38-57}$–His_6 (3 µM) were incubated in PBS containing 20% mouse plasma for 4 h at 37 °C and immediately quenched by the addition of 100×EDTA and 100×protease inhibitor cocktail (Thermo Fisher Scientific). MaxiSorp plates (Thermo Fisher Scientific) were coated overnight with anti-FLAG M2 antibody (Sigma) at 10 µg ml^{-1} and then blocked with PBS containing 2% BSA, 5% non-fat milk and 0.01% Tween-20. Antigen in quenched reaction solution and freshly prepared antigen at equivalent concentration were diluted 200× in blocking buffer + EDTA + protease inhibitor and incubated on the coated ELISA plates for 1.5 h at room temperature. Detection was performed using a horse radish peroxidase (HRP)-conjugated polyclonal rabbit anti-His_6 antibody (Abcam) diluted 1:1,000 in blocking buffer for 1.5 h at 4 °C and developed using TMB (Thermo Fisher Scientific) and sulfuric acid. Separate standards for the peptide and protein analytes were prepared. Wash buffer consisted of PBS + 0.01% Tween-20, and at least three washes were performed between each incubation step.

Biodistribution studies. *IVIS imaging.* FITC-conjugated dextrans of various molecular weights (Sigma), 5-FAM-conjugated peptides (GenScript) or 5/6-FAM-conjugated proteins, in saline or Montanide ISA 51 VG ST formulation (Seppic), were subcutaneously injected at the tail base of B6 mice; the inguinal lymph node was excised 8 h later and imaged on an IVIS Spectrum imaging system (Caliper Life Sciences; excitation, 500 nm; emission, 540 nm). In our analysis of Montanide formulation trafficking (Supplementary Fig. 5), the injection site of the animal was imaged as well. Images were analysed using the Living Image software. Following protein conjugation, the concentration of the labelled protein was calculated using A_{493}. The following dosages were used: Fig. 1f, 2.7 nmol labelled MSA–$E7_{38-57}$ and up to 27 nmol $E7_{38-57}$; Fig. 4b, 2.5 nmol MSA–$E7_{38-57}$ and TTR–$E7_{38-57}$; Supplementary Fig. 5, 1.2 nmol labelled MSA–$E7_{38-57}$ and up to 6 nmol $E7_{38-57}$; and Supplementary Fig. 8f, 0.5 nmol labelled MSA–$E7_{38-57}$ and DEC1–MSA–$E7_{38-57}$.

Cellular biodistribution. Alexa Fluor 488-NHS ester (Thermo Fisher Scientific) was conjugated to recombinantly expressed proteins and injected subcutaneously at the tail base of B6 mice. Following protein conjugation, the concentration of the labelled protein was calculated using A_{495}. The inguinal lymph node was excised 24 h later and processed for single-cell analysis (see the 'Flow cytometry' section). The following dosages were used: Fig. 4c, 2.5 nmol MSA–$E7_{38-57}$ and TTR–$E7_{38-57}$; Supplementary Fig. 8e, 0.5 nmol labelled MSA–$E7_{38-57}$ and DEC1–MSA–$E7_{38-57}$.

Detection of anti-MSA and anti-TTR antibodies. Titrating serum on an analyte-coated ELISA plate is an ineffective way to detect antibodies against serum proteins because of the potential for competition between serum in solution and the analyte on the coated plate surface. Instead, we first purified IgG from serum using Pierce protein A spin plates (Thermo Fisher Scientific), as per the manufacturer's instructions, before detection in ELISA format. MaxiSorp plates (Thermo Fisher Scientific) were coated with 10 µg ml^{-1} MSA (Alpha-Diagnostic International) or TTR (Aviva Systems Biology) overnight and then blocked with PBS containing 0.1% bovine IgG (Sigma) and 0.1% Tween-20 for anti-MSA antibody detection or PBS containing 5% non-fat milk and 0.1% Tween-20 for anti-TTR antibody detection. The IgG eluate from the spin plate was diluted 3× in blocking buffer and then added to the plate for an incubation of 1.5 h at room temperature. Goat anti-mouse HRP-detection antibody (Bio-Rad) was used at a 1:5,000 dilution in blocking buffer and incubated for 1 h at 4 °C. The controls included IgG isolates from Ova-vaccinated animals on wells coated with 10 µg ml^{-1} Ova, and MSA/TTR-coated wells assessed with chicken polyclonal anti-MSA/TTR antibodies (Abcam) and with goat anti-chicken HRP (Abcam) detection, followed by TMB and sulfuric acid development. The wash buffer consisted of PBS containing 0.01% Tween-20, and at least three washes were performed between each incubation step.

Yeast surface display. Fibronectin domains were engineered to bind the DEC-205 ectodomain as previously described[63]. Briefly, the two outermost extracellular domains of DEC-205 (the N-terminal cysteine-rich and type II fibronectin domains) were produced from HEK cells and used to select for binders from the G4 library. Four rounds of magnetic enrichment were followed by seven rounds of flow cytometry-based sorting, with additional diversity introduced through error-prone PCR between sorting rounds. After sorting and sequencing, four individual clones were displayed on yeast, and binding to soluble DEC-205 was measured using flow cytometry to calculate the K_d. DEC1 was measured to have a K_d of 0.66 nM.

Adoptive transfer. $CD8^+$ T cells from $Thy1.1^+$ pmel spleens were isolated using the EasySep mouse $CD8^+$ T-cell isolation kit (STEMCELL Technologies). To assess the kinetics of TCR engagement, we retro-orbitally intravenously transferred 5×10^5 $Thy1.1^+$ pmel cells into animals that had previously been subcutaneously vaccinated with 3 µg peptide equivalence MSA–$gp100_{20-39}$ APL or TTR–$gp100_{20-39}$ APL mixed with 25 µg cyclic di-GMP (InvivoGen) 1, 4 or 7 d earlier. The spleen and inguinal and mesenteric lymph nodes were excised 24 h after the transfer, and the $Thy1.1^+$ cells were assessed for CD69 expression by flow cytometry (see the 'Flow cytometry' section). The AUC calculations were performed using the trapezoidal method. To assess the T-cell phenotype in response to tolerization, $CD8^+$ T cells from $Thy1.1^+$ pmel mice isolated as above and labelled with carboxyfluorescein succinimidyl ester (CFSE; Thermo Fisher Scientific) at a cell density of 1×10^7 cells ml^{-1} and a CFSE concentration of 5 µM for 20 min at 37 °C in PBS containing 0.1% BSA, and subsequently quenched by the addition of FBS. CFSE-labelled $Thy1.1^+$ pmel cells (1×10^6) were retro-orbitally transferred into naive animals in PBS. The recipient mice were intravenously vaccinated 24 h later with 3 µg $gp100_{20-39}$ APL peptide, MSA–$gp100_{20-39}$ or PBS control. The spleen and inguinal and mesenteric lymph nodes were excised 72 h post-immunization, and the $Thy1.1^+$ cells were assessed by flow cytometry (see 'Flow cytometry' section). Proliferation index = $\log_2[FI_{nd}/MFI_{all}]$ where MFI_{al} is the MFI of live $Thy1.1^+$ pmel T cells and FI_{nd} is the peak fluorescence intensity of viable undivided $Thy1.1^+$ pmel T cells.

Tumour studies. TC-1 or B16F10 (3×10^5) cells were subcutaneously administered in 50 µl sterile PBS on the right flank of shaved WT B6 mice, except in Fig. 4h, where 1×10^6 TC-1 cells were implanted. Mice bearing TC-1 tumours were treated on days 5, 12 and 19 (Fig. 2d), and on days 8 and 15 (Fig. 4h); mice bearing B16F10 tumours were vaccinated on days 4, 10 and 16, and/or treated with 200 µg anti-PD1 antibody (clone 29F.1A12, BioXCell) on days 4, 7, 10, 13, 16 and 19. The mice were randomized into groups before treatment initiation. Tumour size was measured by area (longest dimension × perpendicular dimension) and the mice were euthanized when the tumour area exceeded 100 mm^2. Memory from animals vaccinated with $E7_{38-57}$ was assessed by inoculating 3×10^5 TC-1 cells in the mice 66 d post-boost and assessing survival as above.

Statistical analysis. All statistical analyses were performed using the GraphPad Prism software. The specifics of the statistical test performed, *P* values and number of replicates are stated in the figure legends. For all tests, the threshold for significance was $P<0.05$.

Reporting summary. Further information on research design is available in the Nature Research Reporting Summary linked to this article.

Data availability

The main data supporting the findings of this study are available within the paper and its Supplementary information. The associated raw data are too numerous to be readily shared publicly but can be made available from the corresponding author on reasonable request.

Received: 4 April 2019; Accepted: 27 April 2020;
Published online: 01 June 2020

References

1. Garon, E. B. et al. Pembrolizumab for the treatment of non-small-cell lung cancer. *N. Engl. J. Med.* **372**, 2018–2028 (2015).
2. Larkin, J. et al. Combined nivolumab and ipilimumab or monotherapy in untreated melanoma. *N. Engl. J. Med.* **373**, 23–34 (2015).
3. Brahmer, J. R. et al. Safety and activity of anti-PD-L1 antibody in patients with advanced cancer. *N. Engl. J. Med.* **366**, 2455–2465 (2012).
4. Neelapu, S. S. et al. Axicabtagene ciloleucel CAR T-cell therapy in refractory large B-cell lymphoma. *N. Engl. J. Med.* **377**, 2531–2544 (2017).
5. Maude, S. L. et al. Tisagenlecleucel in children and young adults with B-cell lymphoblastic leukemia. *N. Engl. J. Med.* **378**, 439–448 (2018).
6. Kantarjian, H. et al. Blinatumomab versus chemotherapy for advanced acute lymphoblastic leukemia. *N. Engl. J. Med.* **376**, 836–847 (2017).

7. Andtbacka, R. H. I. et al. Talimogene laherparepvec improves durable response rate in patients with advanced melanoma. *J. Clin. Oncol.* **33**, 2780–2788 (2015).
8. Kantoff, P. W. et al. Sipuleucel-T immunotherapy for castration-resistant prostate cancer. *N. Engl. J. Med.* **363**, 411–422 (2010).
9. Snyder, A. et al. Genetic basis for clinical response to CTLA-4 blockade in melanoma. *N. Engl. J. Med.* **371**, 2189–2199 (2014).
10. Rizvi, N. A. et al. Mutational landscape determines sensitivity to PD-1 blockade in non-small cell lung cancer. *Science* **348**, 124–128 (2015).
11. Hodi, F. S. et al. Immunologic and clinical effects of antibody blockade of cytotoxic T lymphocyte-associated antigen 4 in previously vaccinated cancer patients. *Proc. Natl Acad. Sci. USA* **105**, 3005–3010 (2008).
12. Ott, P. A. et al. An immunogenic personal neoantigen vaccine for patients with melanoma. *Nature* **547**, 217–221 (2017).
13. Keskin, D. B. et al. Neoantigen vaccine generates intratumoral T cell responses in phase Ib glioblastoma trial. *Nature* **565**, 234–239 (2019).
14. Liu, H. et al. Structure-based programming of lymph-node targeting in molecular vaccines. *Nature* **507**, 519–522 (2014).
15. McLennan, D. N., Porter, C. J. H. & Charman, S. A. Subcutaneous drug delivery and the role of the lymphatics. *Drug Discov. Today Technol.* **2**, 89–96 (2005).
16. Brinckerhoff, L. H. et al. Terminal modifications inhibit proteolytic degradation of an immunogenic mart-$1_{27–35}$ peptide: implications for peptide vaccines. *Int. J. Cancer* **83**, 326–334 (1999).
17. Moynihan, K. D. et al. Enhancement of peptide vaccine immunogenicity by increasing lymphatic drainage and boosting serum stability. *Cancer Immunol. Res.* **6**, 1025–1038 (2018).
18. Moon, J. J. et al. Interbilayer-crosslinked multilamellar vesicles as synthetic vaccines for potent humoral and cellular immune responses. *Nat. Mater.* **10**, 243–251 (2011).
19. Kuai, R., Ochyl, L. J., Bahjat, K. S., Schwendeman, A. & Moon, J. J. Designer vaccine nanodiscs for personalized cancer immunotherapy. *Nat. Mater.* **16**, 489–496 (2017).
20. Nembrini, C. et al. Nanoparticle conjugation of antigen enhances cytotoxic T-cell responses in pulmonary vaccination. *Proc. Natl Acad. Sci. USA* **108**, E989–E997 (2011).
21. Bonifaz, L. C. et al. In vivo targeting of antigens to maturing dendritic cells via the DEC-205 receptor improves T cell vaccination. *J. Exp. Med.* **199**, 815–824 (2004).
22. Kretz-Rommel, A. et al. In vivo targeting of antigens to human dendritic cells through DC-SIGN elicits stimulatory immune responses and inhibits tumor growth in grafted mouse models. *J. Immunother.* **30**, 715–726 (2007).
23. Johansen, P. et al. Direct intralymphatic injection of peptide vaccines enhances immunogenicity. *Eur. J. Immunol.* **35**, 568–574 (2005).
24. Jewell, C. M., Bustamante Lopez, S. C. & Irvine, D. J. In situ engineering of the lymph node microenvironment via intranodal injection of adjuvant-releasing polymer particles. *Proc. Natl Acad. Sci. USA* **108**, 15745–15750 (2011).
25. Supersaxo, A., Hein, W. R. & Steffen, H. Effect of molecular weight on the lymphatic absorption of water-soluble compounds following subcutaneous administration. *Pharm. Res.* **7**, 167–169 (1990).
26. Feltkamp, M. C. W. et al. Vaccination with cytotoxic T lymphocyte epitope-containing peptide protects against a tumor induced by human papillomavirus type 16-transformed cells. *Eur. J. Immunol.* **23**, 2242–2249 (1993).
27. Hailemichael, Y. et al. Persistent antigen at vaccination sites induces tumor-specific $CD8^+$ T cell sequestration, dysfunction and deletion. *Nat. Med.* **19**, 465–472 (2013).
28. Burdette, D. L. et al. STING is a direct innate immune sensor of cyclic di-GMP. *Nature* **478**, 515–518 (2011).
29. Guevara-Patiño, J. A. et al. Optimization of a self antigen for presentation of multiple epitopes in cancer immunity. *J. Clin. Invest.* **116**, 1382–1390 (2006).
30. van Stipdonk, M. J. B. et al. Design of agonistic altered peptides for the robust induction of CTL directed towards $H\text{-}2D^b$ in complex with the melanoma-associated epitope gp100. *Cancer Res.* **69**, 7784–7792 (2009).
31. Mennuni, C. et al. Efficient induction of T-cell responses to carcinoembryonic antigen by a heterologous prime-boost regimen using DNA and adenovirus vectors carrying a codon usage optimized cDNA. *Int. J. Cancer* **117**, 444–455 (2005).
32. Han, S., Asoyan, A., Rabenstein, H., Nakano, N. & Obst, R. Role of antigen persistence and dose for $CD4^+$ T-cell exhaustion and recovery. *Proc. Natl Acad. Sci. USA* **107**, 20453–20458 (2010).
33. Ramsdell, F. & Fowlkes, B. J. Maintenance of in vivo tolerance by persistence of antigen. *Science* **257**, 1130–1134 (1992).
34. Ehl, S. et al. Antigen persistence and time of T-cell tolerization determine the efficacy of tolerization protocols for prevention of skin graft rejection. *Nat. Med.* **4**, 1015–1019 (1998).
35. Warren, K. G., Catz, I., Ferenczi, L. Z. & Krantz, M. J. Intravenous synthetic peptide MBP8298 delayed disease progression in an HLA class II-defined cohort of patients with progressive multiple sclerosis: results of a 24-month double-blind placebo-controlled clinical trial and 5 years of follow-up treatment. *Eur. J. Neurol.* **13**, 887–895 (2006).
36. Bielekova, B. et al. Encephalitogenic potential of the myelin basic protein peptide (amino acids 83–99) in multiple sclerosis: Results of a phase II clinical trial with an altered peptide ligand. *Nat. Med.* **6**, 1167–1175 (2000).
37. Hanson, M. C. et al. Nanoparticulate STING agonists are potent lymph node–targeted vaccine adjuvants. *J. Clin. Invest.* **125**, 2532–2546 (2015).
38. Churlaud, G. et al. Human and mouse $CD8^+CD25^+FOXP3^+$ regulatory T cells at steady state and during interleukin-2 therapy. *Front. Immunol.* **6**, 171 (2015).
39. Yu, Y. et al. Recent advances in $CD8^+$ regulatory T cell research. *Oncol. Lett.* **15**, 8137–8194 (2018).
40. Tsai, S., Clemente-Casares, X. & Santamaria, P. $CD8^+$ Tregs in autoimmunity: learning 'self'-control from experience. *Cell. Mol. Life Sci.* **68**, 3781–3795 (2011).
41. Ingenbleek, Y. & Young, V. Transthyretin (prealbumin) in health and disease: nutritional implications. *Annu. Rev. Nutr.* **14**, 495–533 (1994).
42. Terje Andersen, J., Bekele Daba, M., Berntzen, G., Michaelsen, T. E. & Sandlie, I. Cross-species binding analyses of mouse and human neonatal Fc receptor show dramatic differences in immunoglobulin G and albumin binding. *J. Biol. Chem.* **285**, 4826–4836 (2010).
43. McCutchen, S. L., Colon, W. & Kelly, J. W. Transthyretin mutation Leu-55-Pro significantly alters tetramer stability and increases amyloidogenicity. *Biochemistry* **32**, 12119–12127 (1993).
44. Prior, I. A., Lewis, P. D. & Mattos, C. A comprehensive survey of ras mutations in cancer. *Cancer Res.* **72**, 2457–2467 (2012).
45. Waters, A. M. & Der, C. J. KRAS: the critical driver and therapeutic target for pancreatic cancer. *Cold Spring Harb. Perspect. Med.* **8**, a031435 (2018).
46. Bender, S. et al. Reduced H3K27me3 and DNA hypomethylation are major drivers of gene expression in K27M mutant pediatric high-grade gliomas. *Cancer Cell* **24**, 660–672 (2013).
47. Schwartzentruber, J. et al. Driver mutations in histone H3.3 and chromatin remodelling genes in paediatric glioblastoma. *Nature* **482**, 226–231 (2012).
48. Ochs, K. et al. K27M-mutant histone-3 as a novel target for glioma immunotherapy. *Oncoimmunology* **6**, e1328340 (2017).
49. Wang, Q. J. et al. Identification of T-cell receptors targeting KRAS-mutated human tumors. *Cancer Immunol. Res.* **4**, 204–214 (2016).
50. Chheda, Z. S. et al. Novel and shared neoantigen derived from histone 3 variant H3.3K27M mutation for glioma T cell therapy. *J. Exp. Med.* **215**, 141–157 (2018).
51. Zom, G. G. et al. Efficient induction of antitumor immunity by synthetic Toll-like receptor ligand–peptide conjugates. *Cancer Immunol. Res.* **2**, 756–764 (2014).
52. Qiu, F. et al. Poly(propylacrylic acid)-peptide nanoplexes as a platform for enhancing the immunogenicity of neoantigen cancer vaccines. *Biomaterials* **182**, 82–91 (2018).
53. Deng, L. et al. Heterosubtypic influenza protection elicited by double-layered polypeptide nanoparticles in mice. *Proc. Natl Acad. Sci. USA* **115**, E7758–E7767 (2018).
54. Harris, J. R. & Markl, J. Keyhole limpet hemocyanin (KLH): a biomedical review. *Micron* **30**, 597–623 (1999).
55. Kim, S. K. et al. Comparison of the effect of different immunological adjuvants on the antibody and T-cell response to immunization with MUC1-KLH and GD3-KLH conjugate cancer vaccines. *Vaccine* **18**, 597–603 (1999).
56. Lynn, G. M. et al. In vivo characterization of the physicochemical properties of polymer-linked TLR agonists that enhance vaccine immunogenicity. *Nat. Biotechnol.* **33**, 1201–1210 (2015).
57. Wu, T. Y.-H. et al. Rational design of small molecules as vaccine adjuvants. *Sci. Transl. Med.* **6**, 263ra160 (2014).
58. Duperret, E. K. et al. A synthetic DNA, multi-neoantigen vaccine drives predominately MHC class I $CD8^+$ T-cell responses, impacting tumor challenge. *Cancer Immunol. Res.* **7**, 174–182 (2019).
59. Walters, J. N. et al. A novel DNA vaccine platform enhances neo-antigen-like T-cell responses against WT1 to break tolerance and induce anti-tumor immunity. *Mol. Ther.* **25**, 976–988 (2017).
60. Geall, A. J. et al. Nonviral delivery of self-amplifying RNA vaccines. *Proc. Natl Acad. Sci. USA* **109**, 14604–14609 (2012).
61. Horton, H. M. et al. Potent in vitro and in vivo activity of an Fc-engineered anti-CD19 monoclonal antibody against lymphoma and leukemia. *Cancer Res.* **68**, 8049–8057 (2008).
62. Nomura, L. E., Walker, J. M. & Maecker, H. T. Optimization of whole blood antigen-specific cytokine assays for $CD4^+$ T cells. *Cytometry* **40**, 60–68 (2000).
63. Chen, T. F., de Picciotto, S., Hackel, B. J. & Wittrup, K. D. Engineering Fibronectin-Based binding proteins by yeast surface display. *Methods Enzymol.* **523**, 303–326 (2013).

Acknowledgements

We thank the Koch Institute Swanson Biotechnology Center, particularly the Flow Cytometry and Animal Imaging and Preclinical Testing Core Facilities, as well as the Biophysical Instrumentation Facility for technical support. This work was supported, in

part, by the National Institutes of Health (grant no. CA174795 and the National Institute of General Medical Sciences-NIH Interdepartmental Biotechnology Training Program). D.J.I. is an investigator of the Howard Hughes Medical Institute.

Author contributions

N.K.M., K.D.W. and D.J.I. designed the studies and wrote the manuscript. N.K.M., R.V.P. and A.P.S. carried out experiments. K.D.M., A.M.R., N.M. and K.R. assisted with experiments. J.M.-F. provided the DEC-205 binders. S.N.B. lent expertise to the tolerization studies.

Competing interests

D.J.I., K.D.W., N.K.M. and K.R. are inventors on a related patent that covers the primary technology outlined in the manuscript. Massachusetts Institute of Technology is the assignee for this patent application. Application number: US15/452,266. D.J.I. has ownership interest in and is a consultant/advisory board member for Elicio Therapeutics. The remaining authors report no competing interests.

Additional information

Supplementary information is available for this paper at https://doi.org/10.1038/s41551-020-0563-4.

Correspondence and requests for materials should be addressed to K.D.W. or D.J.I.

nature research

Corresponding author(s): Darrell J. Irvine and K. Dane Wittrup

Last updated by author(s): Mar 28, 2020

Reporting Summary

Nature Research wishes to improve the reproducibility of the work that we publish. This form provides structure for consistency and transparency in reporting. For further information on Nature Research policies, see Authors & Referees and the Editorial Policy Checklist.

Statistics

For all statistical analyses, confirm that the following items are present in the figure legend, table legend, main text, or Methods section.

n/a	Confirmed	
☐	☒	The exact sample size (*n*) for each experimental group/condition, given as a discrete number and unit of measurement
☐	☒	A statement on whether measurements were taken from distinct samples or whether the same sample was measured repeatedly
☐	☒	The statistical test(s) used AND whether they are one- or two-sided *Only common tests should be described solely by name; describe more complex techniques in the Methods section.*
☒	☐	A description of all covariates tested
☐	☒	A description of any assumptions or corrections, such as tests of normality and adjustment for multiple comparisons
☐	☒	A full description of the statistical parameters including central tendency (e.g. means) or other basic estimates (e.g. regression coefficient) AND variation (e.g. standard deviation) or associated estimates of uncertainty (e.g. confidence intervals)
☐	☒	For null hypothesis testing, the test statistic (e.g. *F*, *t*, *r*) with confidence intervals, effect sizes, degrees of freedom and *P* value noted *Give P values as exact values whenever suitable.*
☒	☐	For Bayesian analysis, information on the choice of priors and Markov chain Monte Carlo settings
☒	☐	For hierarchical and complex designs, identification of the appropriate level for tests and full reporting of outcomes
☒	☐	Estimates of effect sizes (e.g. Cohen's *d*, Pearson's *r*), indicating how they were calculated

Our web collection on statistics for biologists contains articles on many of the points above.

Software and code

Policy information about availability of computer code

Data collection	No software was used during data collection.
Data analysis	FlowJo Version 9 was used to analyse flow-cytometry data. FIJI was used for image analysis. GraphPad prism was used to plot the figures and to conduct statistical analyses.

For manuscripts utilizing custom algorithms or software that are central to the research but not yet described in published literature, software must be made available to editors/reviewers. We strongly encourage code deposition in a community repository (e.g. GitHub). See the Nature Research guidelines for submitting code & software for further information.

Data

Policy information about availability of data

All manuscripts must include a data availability statement. This statement should provide the following information, where applicable:

- Accession codes, unique identifiers, or web links for publicly available datasets
- A list of figures that have associated raw data
- A description of any restrictions on data availability

The main data supporting the findings of this study are available within the paper and its Supplementary Information files. The associated raw data are too numerous to be readily shared publicly, but can be made available from the corresponding author on reasonable request.

Field-specific reporting

Please select the one below that is the best fit for your research. If you are not sure, read the appropriate sections before making your selection.

☒ Life sciences ☐ Behavioural & social sciences ☐ Ecological, evolutionary & environmental sciences

For a reference copy of the document with all sections, see nature.com/documents/nr-reporting-summary-flat.pdf

Life sciences study design

All studies must disclose on these points even when the disclosure is negative.

Sample size	No sample-size calculation was performed to power each study. Sample sizes were determined on the basis of prior experience with similar studies. Sample sizes were sufficient given the large differences in T cell responses observed between the various tested fusion vaccines.
Data exclusions	Data points were excluded only if 1) faulty injections were noted during experimental execution or 2) in tumor studies if mice were euthanized for reasons unrelated to tumor area (that is, poor body-condition score).
Replication	No studies have been reported that failed upon repeat. Studies that were repeated are noted in figure captions, and include all studies that demonstrate the primary principles reported in the manuscript.
Randomization	In non-tumour bearing mice, there were no attempts at binning naive animals. In therapeutic tumour studies, mice were randomly binned into experimental groups on the day of the first treatment.
Blinding	Because the same individual planned and executed the study, blinding was not performed.

Reporting for specific materials, systems and methods

We require information from authors about some types of materials, experimental systems and methods used in many studies. Here, indicate whether each material, system or method listed is relevant to your study. If you are not sure if a list item applies to your research, read the appropriate section before selecting a response.

Materials & experimental systems

n/a	Involved in the study
☐	☒ Antibodies
☐	☒ Eukaryotic cell lines
☒	☐ Palaeontology
☐	☒ Animals and other organisms
☒	☐ Human research participants
☒	☐ Clinical data

Methods

n/a	Involved in the study
☒	☐ ChIP-seq
☐	☒ Flow cytometry
☒	☐ MRI-based neuroimaging

Antibodies

Antibodies used	BioLegend: CD16/32 (Fc block, clone 93), CD8α (53-6.7), TNF-α (MP6-XT22), IFN-γ (XMG1.2), CD3 (17a2), B220 (RA3-6B2), CD11b (M1/70), CD11c (N418), F4/80 (BM8), CD69 (H1.2F3), CD86 (GL-1), PD1 (29F.1A12), Lag3 (C9B7W), and Tim3 (RMT3-23).
Validation	We used commercially available antibody clones that are routinely used for the purposes of the studies reported in the paper. Pilot experiments were performed to ensure appropriate staining in positive controls. Manufacturers released certificates of analysis for each lot used in these studies.

Eukaryotic cell lines

Policy information about cell lines

Cell line source(s)	HEK – Thermo Fisher Scientific; TC-1 – T.C. Wu (JHU); B16F10 – ATCC
Authentication	None of the cell lines were authenticated.
Mycoplasma contamination	All cell lines tested negative for mycoplasma contamination.
Commonly misidentified lines (See ICLAC register)	No commonly misidentified lines were used in this study.

Animals and other organisms

Policy information about studies involving animals; ARRIVE guidelines recommended for reporting animal research

Laboratory animals	B6 mice (C57BL/6NTac) and HLA-A11 mice (B6-Tg(HLA-A*1101/H2-Kb)A11.01) were purchased from Taconic. Batf3-/- mice (B6.129S(C)-Batf3tm1Kmm/J), pmel Thy1.1+ mice (B6.Cg-Thy1a/Cy Tg(TcraTcrb)8Rest/J), and HLA-A2 mice (C57BL/6-Mcph1Tg(HLA-A2.1)1Enge/J) were purchased from the Jackson Laboratory. OTI mice (C57BL/6-Tg(TcraTcrb)1100Mjb/J) and Thy1.1 mice (B6.PL-Thy1a/CyJ) were purchased from Jackson Laboratory and crossed to generate an OTI Thy1.1+ colony.
Wild animals	The study did not involve wild animals.
Field-collected samples	The study did not involve samples collected from the field.
Ethics oversight	All studies were approved by the MIT Committee on Animal Care (CAC).

Note that full information on the approval of the study protocol must also be provided in the manuscript.

Flow Cytometry

Plots

Confirm that:

☒ The axis labels state the marker and fluorochrome used (e.g. CD4-FITC).

☒ The axis scales are clearly visible. Include numbers along axes only for bottom left plot of group (a 'group' is an analysis of identical markers).

☒ All plots are contour plots with outliers or pseudocolor plots.

☒ A numerical value for number of cells or percentage (with statistics) is provided.

Methodology

Sample preparation	Details of sample preparation are provided in Methods, including tissue-processing steps. Briefly, lymph nodes were digested in studies to analyse dendritic-cell populations; otherwise, tissues were processed by the mechanical generation of single-cell suspensions.
Instrument	BD FACSCanto and BD FACS LSR Fortessa.
Software	FlowJo v9
Cell population abundance	The relative abundance of each gate is shown in Supplementary Fig. 9.
Gating strategy	The gating strategy is outlined in Supplementary Fig. 9.

☒ Tick this box to confirm that a figure exemplifying the gating strategy is provided in the Supplementary Information.